FUNDAMENTAL STUDIES ON SILICON DIOXIDE CHEMICAL MECHANICAL POLISHING

By

UDAY MAHAJAN

A DISSERTATION PRESENTED TO THE GRADUATE SCHOOL
OF THE UNIVERSITY OF FLORIDA IN PARTIAL FULFILLMENT
OF THE REQUIREMENTS FOR THE DEGREE OF
DOCTOR OF PHILOSOPHY

UNIVERSITY OF FLORIDA

2000

To my parents

ACKNOWLEDGMENTS

I would like to acknowledge many people that have made this work possible and made my stay in Gainesville a pleasant one. Firstly, I would like to express my heartfelt appreciation to my advisor, Dr. Rajiv K. Singh, for his guidance, support, and encouragement. He always gave me freedom to try out various ideas and gave me several valuable suggestions, which helped me to learn more and also taught me the importance of thinking creatively. Thanks are also due to my doctoral committee members, Dr. Cammy Abernathy, Dr. Brij Moudgil, Dr. Stephen Pearton and Dr. Dinesh Shah, for their interest and assistance in this work.

I would like to acknowledge the Engineering Research Center for Particle Science and Technology for its support. I would also like to acknowledge the help of Gill Brubaker, who was of great help in teaching me to use several ERC instruments, and also at troubleshooting various problems along the way. I would also like to thank the student members of the ERC for their constructive advice and help at various stages of this work. Thanks go to Bahar, Byron, Josh, Pankaj and Seung-Mahn. Special thanks are due to Dr. Dong-Gu Lee, who

helped me in many ways during his stay as a graduate student. The MAIC staff was also very helpful in teaching and troubleshooting their equipment.

On a more personal note, I would also like to acknowledge my group members and other friends, who made graduate school a very pleasant experience. Thanks go to Dr. Ali Ata, Anu (Lieutenant), Anupam (Rinku), Arul, Dr. Don Gilbert, Dr. Dong-Gu Lee, Frank, Hui, Jadeja, Jeremiah, Dr. Jim Fitzgerald, Josh (Jose), Krau (K-man), Dr. Dhananjay Kumar, Kyo-Sei (Godfather), Dr. Kyu-Gong Cho, Marc, Mike (Molli), Nabil (Niobium), Nagraj, Pankaj (Punk), Dr. Ramesh Raghunathan, Rajesh, Dr. Ravi Adimula, Sai, Dr. Mohamed Saleem, Sandeep, Sanjeeb, Seung-Mahn, Srini (Nole), Subra, Dr. Valentin Craciun, Won-Seok, Won-Seop, Zhan (Sabee) and many others. I would also like to thank my friends from my undergraduate days and Mr. Samuel Adams, Johnnie Walker and Senór Corona for their loyal friendship over the years.

Finally, I must express my deepest appreciation to my parents and sister, whose love and encouragement have enabled me to achieve all my accomplishments in life so far.

TABLE OF CONTENTS

Page

ACKNOWLEDGMENTS iii

LIST OF TABLES viii

LIST OF FIGURES ix

ABSTRACT xiii

CHAPTERS

1 INTRODUCTION 1
  Motivation and Objectives 1
  Dissertation Outline 4

2 LITERATURE SURVEY 7

  Advanced Metallization 7
    Impact of Interconnect Delay on Performance . . . 7
    Methods of Reducing Interconnect Delay 9
    Multilevel Metallization 9
    Planarization 11
      Planarization requirements 11
      Planarization techniques 12
      Advantages of CMP 13
      Disadvantages of CMP 14
  Chemical and Mechanical Effects in CMP 15
    Mechanical Abrasion 16
      Effect of particle size 18
      Theories of removal rate 20
      Polishing pad 21
    Chemical Effects in Metal CMP 23
      Tungsten CMP 25
      Aluminum CMP 28
      Copper CMP 32
    CMP of Silicon Dioxide 38
      Role of water in glass (SiO_2) polishing . . 40
      Interaction between abrasive particles and oxide

surface 43
SiO_2 CMP in Microelectronics Manufacturing . 46
CMP of Low Dielectric Constant Materials 49
Scope of This Dissertation 53

3 IN-SITU FRICTION FORCE MEASUREMENTS 66

Introduction 66
Materials and Methods 67
Setup of Instrument 67
Atomic Force Microscopy (AFM) 68
Results and Discussion 70
Effect of Surface Roughness 70
Solution Chemistry Effects for SiO_2 74
Effect of Pressure and Velocity 77
Summary 79

4 EFFECT OF PARTICLE SIZE 93

Introduction 93
Materials and Methods 93
Ellipsometry 94
Slurry Preparation 96
Particle Size Analysis 96
Setup for Polishing 97
Results and Discussion 99
Experimental Results 99
Polishing rate 99
Surface morphology of polished samples . . 100
Theoretical Model 102
Mechanical removal 103
Chemical modification of surface 105
Contact area 109
Summary 110

5 EFFECT OF SLURRY IONIC STRENGTH 123

Introduction 123
Materials and Methods 124
Particle Size Analysis 124
Zeta Potential 126
Turbidity Measurements 128
Results and Discussion 129
Polishing Rate and Surface Morphology 129
Zeta Potential, Turbidity and Particle Size . . 130
Summary 134

6 EFFECT OF ABRASIVE MATERIAL PROPERTIES 141

Introduction 141
Materials and Methods 142
Results and Discussion 146
    Effect of Abrasive Density 146
    Effect of Abrasive Material 150
Summary 154

7 CONCLUSIONS 167

LIST OF REFERENCES 171

BIOGRAPHICAL SKETCH 178

LIST OF TABLES

Table Page

- 4.1: Average number of pits, pit diameter and pit depth for samples polished with 15.0 wt.% slurries of the four different particle sizes used in this study . . . 101
- 6.1: Properties of alumina particles of different densities 147
- 6.2: Properties of the different phases present in the alumina particles [Git70] 147
- 6.3: Properties of different powders used in this study 150

LIST OF FIGURES

Figure Page

- 1.1: Schematic outline of CMP Process 6
- 2.1: Capacitance associated with metal lines as a function of feature size [Jen94] 54
- 2.2: Gate delay and Interconnect delay as a function of minimum feature size [Jen94] 55
- 2.3: Cross-section of Multi Level Metallization (MLM) Scheme [Sti97] 56
- 2.4: Degrees of Planarity (a) Unplanarized (b) Surface Smoothing (c) Local Planarization (d) Global Planarization [Ols93] 57
- 2.5: Schematic illustration of dishing and erosion [Sin00] 58
- 2.6: (a) New and (b) glazed Suba IV pad [Ste97] . . 59
- 2.7: Process flow for a dual damascene Copper Interconnect Process [Jac98] 60
- 2.8: Polishing rate of various glasses as a function of (a) Vickers Microhardness (b) Softening Point and (c) Weight loss in water [Izu79] 61
- 2.9: Polishing rate of various glasses as a function of Vickers Microhardness for (a) Oil Polishing (b) Dry Polishing [Izu79] 62
- 2.10: Penetration of different liquids into a glass surface during indentation [Hir87] 63
- 2.11: Polishing rate of various abrasives as a function of their Isoelectric Point (IEP) [Kal62], [Sil82] . 64
- 2.12: Schematic illustration of STI CMP Process [Ste97]

. . . . 65

- 3.1: Schematic outline of Friction Force Measurement Apparatus 81
- 3.2: AFM Micrographs of Silica films of two different roughnesses 82
- 3.3: Friction force response for silica surfaces of two different roughnesses 83
- 3.4: AFM Micrographs of unpolished and polished Tungsten surfaces before the friction measurements 84
- 3.5: Friction force response for rough (unpolished) and smooth (polished) Tungsten films 85
- 3.6: AFM Micrograph of rough Tungsten surface after the friction experiments 86
- 3.7: Section analysis of Tungsten film (a) before and (b) after the friction experiments 87
- 3.8: Effect of solution pH on friction forces for Silica 88
- 3.9: Effect of solution Ionic Strength on friction forces for Silica 89
- 3.10: Friction force for Silica as a function of applied pressure 90
- 3.11: Friction force as a function of pad velocity for new and degraded pads 91
- 3.12: Stribeck curve, showing variation of friction coefficient with velocity for surfaces with two different roughnesses [McG74] 92
- 4.1: (a)Setup for the polishing experiments (b) Schematic of sample holder used for polishing 112
- 4.2: Electron Micrographs of (A) 0.2 µm (B) 0.5 µm (C) 1.0 µm and (D) 1.5 µm diameter SiO_2 particles . . 113
- 4.3: Size distributions for SiO_2 particles obtained by Dynamic Light Scattering 114

- 4.4: SiO_2 polishing rates as a function of solids loading for 0.2, 0.5, 1.0 and 1.5 µm diameter SiO_2 particles 115
- 4.5: AFM micrographs and sections of samples polished with 2.0 wt.% slurries of SiO_2 particles 116
- 4.6: AFM micrographs and sections of samples polished with 15.0 wt.% slurries of SiO_2 particles 117
- 4.7: Calculated Total Indent Volume as a function of concentration for different particle sizes 118
- 4.8: Calculated Diffusion depth of water as a function of concentration for different particle sizes 119
- 4.9: Calculated total modified volume as a function of concentration for different particle sizes 120
- 4.10: Calculated Contact area between particles and wafer as a function of concentration for different particle sizes 121
- 4.11: Calculated surface area of particles as a function of concentration for different particle sizes . . 122
- 5.1: Schematic illustration of Acoustosizer [OBr95] 135
- 5.2: SiO_2 Polishing Rate as a function of salt concentration for LiCl, NaCl and KCl 136
- 5.3: RMS roughness of polished samples for different salt concentrations 137
- 5.4: Zeta Potential as a function of Ionic Strength for SiO_2 suspensions containing LiCl, NaCl and KCl . . 138
- 5.5: Normalized turbidity of SiO_2 suspensions containing 1.0 M salt as a function of time 139
- 5.6: Particle size distribution of SiO_2 suspensions containing 1.0 M Salt (Inset: Particle size distribution of stable suspension) 140
- 6.1: Thermal transformation characteristics of Alumina [Git70] 155
- 6.2: Specific surface area of Alumina particles as a

function of particle density 156

- 6.3: TEM Micrographs of Alumina particles from samples A, B, C and D 157
- 6.4: SiO_2 polishing rate as a function of Alumina particle density for pH 4 and 11 158
- 6.5: AFM Micrographs of samples polished with Alumina slurries at pH 4 159
- 6.6: AFM Micrographs of samples polished with Alumina slurries at pH 11 160
- 6.7: (a) SiO_2 polishing rate as a function of Al_2O_3 slurry pH (b) Zeta Potential of Al_2O_3 particles as a function of pH 161
- 6.8: XPS surface analysis of residual Alumina on wafer surface after polishing at different pHs 162
- 6.9: (a) SiO_2 polishing rate as a function of TiO_2 slurry pH (b) Zeta Potential of TiO_2 particles as a function of pH 163
- 6.10: (a) SiO_2 polishing rate as a function of ZrO_2 slurry pH (b) Zeta Potential of ZrO_2 particles as a function of pH 164
- 6.11: SEM micrographs of wafer surfaces after polishing with (a) Alumina and (b) Titania particles at their respective IEPs 165
- 6.12: (a) SiO_2 polishing rate as a function of SiO_2 slurry pH (b) Zeta Potential of SiO_2 particles as a function of pH 166

Abstract of Dissertation Presented to the Graduate School
of the University of Florida in Partial Fulfillment of the
Requirements for the Degree of Doctor of Philosophy

FUNDAMENTAL STUDIES ON SILICON DIOXIDE CHEMICAL MECHANICAL POLISHING

By

Uday Mahajan

December, 2000

Chairperson: Dr. Rajiv K. Singh
Major Department: Materials Science and Engineering

Chemical Mechanical Polishing (CMP) has lately been adopted on a large scale by the semiconductor industry for planarizing and patterning metal and dielectric films. Additionally, CMP has been used for hundreds of years for optical polishing. Still, several aspects of this process remain poorly understood. In this study, some results on CMP of SiO_2 are presented with a view to characterizing the effects of abrasive properties and slurry chemistry on the polishing process. Additionally, some results from a novel in-situ friction force measuring instrument are also presented.

The friction force results showed the effect of several parameters such as surface roughness, solution pH and ionic strength on wafer-pad interactions. Additionally, monitoring the friction as a function of velocity showed that the transition from boundary lubrication to full fluid-film lubrication depends on the roughness (conditioning) of the polishing pad.

The parameters investigated in the polishing experiments include abrasive size and concentration. From the experimental results, it was found that an optimum concentration exists for each abrasive size, which shifts to lower values and becomes narrower as particle size increases. From calculations, this was attributed to a decreased ability of the large particles to chemically modify the surface of the SiO_2 films. The smaller particles, having a much larger surface area, are able to better adsorb dissolution and abrasion products at high concentrations, thus leading to high removal rates under those conditions.

Studies on the effect of slurry ionic strength showed that the ability of a metal ion to shield the surface charge on the surfaces interacting during polishing is what determined the removal rate. This was due to the reduced electrostatic repulsion between the surfaces, which resulted in better contact and thus higher polishing rates. These results were corroborated by the earlier friction force measurements.

Finally, the influence of particle density on polishing was shown, with denser alumina particles being able to polish SiO_2 much more effectively. Some preliminary results on polishing with different abrasives as a function of slurry pH indicate that the material properties of the abrasives seem to change around their Iso-electric Points (IEP), resulting in almost no polishing, and severe particle contamination on the SiO_2 surface.

CHAPTER 1
INTRODUCTION

Motivation and Objectives

Chemical Mechanical Polishing, as the name suggests, involves the utilization of chemical reactions and mechanical (abrasive) wear to polish surfaces. This process has been used in different forms for more than a thousand years to polish a wide variety of materials, from optically flat and smooth mirror surfaces to metal inlaid objects prepared by the so-called "Damascene" process. In recent times, extremely smooth and flat glass and semiconductor(wafer) surfaces have been obtained by using CMP processes. In modern microprocessors, increasing device densities and shrinking feature sizes have led to the adoption of multilevel interconnection technologies. CMP has emerged as the most effective technique for achieving global planarization of the metal and dielectric layers in these multilevel metallization schemes [Ste97]. In this process, schematically illustrated in Figure 1.1, the rotating wafer surface is held against a rotating polishing pad, which is soaked with the polishing slurry. The slurry contains chemical reagents, which create an easily removable surface layer on the material to be planarized, which is then removed by the mechanical action of the abrasive particles. The means by which planarization is achieved with CMP is to maintain high removal rates at the high surface features and low removal rates at the low surface features. For this purpose, a rigid and incompressible polishing pad is used, which exerts a significant force on the high features, resulting in high removal rates, but since it does not conform to the entire wafer surface, it does not exert force on the low features. So far, CMP has been used to planarize dielectrics and metals of several types, e.g. SiO_2, Si_3N_4, tungsten, copper, and aluminum. In IC fabrication, precise control of the polishing process is required, as very thin layers (sometimes less than 0.5 μm) have to be removed in a precisely controlled manner. Many times the process ends when the material being polished is entirely removed, and it is important that the underlying structures not be damaged. In spite of all these problems, CMP is still by far the most preferred technique for planarization, and is one of the fastest growing sectors in the IC manufacturing industry [Oma98]. With the advent of copper interconnect technology and the increasing use of Shallow Trench Isolation (STI) for isolating transistors, it is being used more widely than ever.

Despite its widespread use, there is only a limited amount of information available about the fundamental polishing mechanisms underlying the process. The main components of the CMP process are the wafer surface (which is to be polished), polishing pad and the polishing slurry. These components have several parameters, which interact with each other in different ways and have to be properly controlled in order to achieve an optimum polishing process. Most polishing models that have been developed so far [Run94], [Yu93] are based on old studies done on glass polishing [Pre27],which treat CMP as a primarily mechanical process. Parameters like slurry flow dynamics, polishing pad properties and substrate geometry are considered, but abrasive and slurry properties are often neglected. Some important parameters that need further study include particle size, shape, concentration and material. Slurry chemistry parameters like pH and ionic strength, and how these affect stability and polishing behavior, also need to be more fully understood. A systematic evaluation of the effects of these parameters will not only shed light on the mechanics of polishing, but will also help in designing processes for present and next generation processes. Additionally, there is a need to develop in-situ characterization techniques to study wafer-slurry-pad interactions, which can be useful for process understanding as well as for developing process control and end-point detection techniques.

Dissertation Outline

Chapter 2 presents a general review on the subject of multilevel metallization (MLM), metal and oxide CMP and glass polishing, and summarizes the previous work in this field. This includes a brief explanation of the reasons for introducing MLM, and a description of other planarization techniques used in IC manufacturing, prior to the introduction of CMP. Current processes, such as tungsten, copper and aluminum CMP, are briefly described as well. Oxide CMP, the main focus of this research, is described in more detail, with a summary of the mechanisms of glass (SiO_2)dissolution and polishing, which forms the basis of most knowledge in this area.

Chapter 3 deals with an in-situ friction force measurement technique that was developed as a part of this project. The principles of operation are briefly described, along with some of the characterization tools used in this study. Following this, some of the results are presented. The variation of friction with surface roughness, solution chemistry and polishing pad condition is shown. Chapter 4 deals with the effect of slurry particle size on oxide polishing. The experimental procedures and characterization methods that were used to prepare the polishing slurries and for conducting the polishing experiments are discussed. A simple analytical model to explain the experimental data is also described. Chapter 5 presents and discusses the results of the oxide polishing experiments as a function of slurry ionic strength, correlating the polishing and slurry stability results to the friction force experiments which are described in Chapter 3. Chapter 6 presents some initial results on the effect of abrasive properties on oxide CMP. The effect of the density of the particles is shown, along with some preliminary results on the effect of abrasive chemistry (Iso-electric point, nature of abrasive).

The conclusions of these studies, along with recommendations for future work, are presented in Chapter 7.

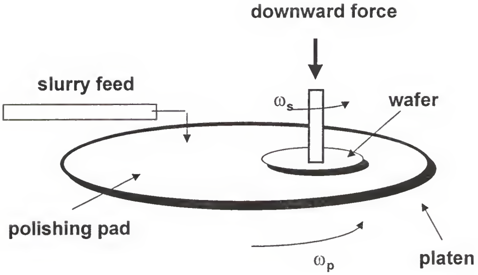

Figure 1.1: Schematic outline of CMP Process

CHAPTER 2
LITERATURE SURVEY

Advanced Metallization

Advanced metallization technologies have become critically important to obtain the performance benefits of scaling device dimensions to the sub-0.5 μm regime. This reduction in feature size has had an adverse effect on interconnection performance, as a result of which new technologies such as low resistivity metals, low-k dielectrics and Multilevel Metallization (MLM) have been introduced.

Impact of Interconnect Delay on Performance

Interconnect delays in integrated circuits are due to the resistance (R) and capacitance (C) associated with the metal lines. The RC time delay, which is the time taken by the voltage at one end of the line to reach 63% of its final value when a step input is applied at the other end of the line [Ste97] is used as an index of interconnect delay. The RC time delay is equal to the product of the total resistance and capacitance of the metal line. The higher the value of RC, the slower the operating speed of the device. The expression for RC is

$$RC = \rho\varepsilon_{ox}\frac{L^{2}}{t_{ox}d} \qquad (2.1)$$

where L, d and ρ are the length, thickness and resistivity of the metal line, and ϵ_{ox} and t_{ox} are the Inter Level Dielectric (ILD) permittivity and thickness respectively. Therefore, to reduce the RC time delay, ϵ_{ox}, ρ and L must be reduced, and D and t_{ox} must be increased. The above equation also suggests that RC delay is independent of line width, and therefore should not change as line dimensions are reduced. However, when feature sizes are reduced, the line thickness and ILD thickness are scaled down, but often the line length remains constant. As a result, RC delay increases.

Another factor causing an increase in RC delay is that equation 2.1 only considers line-to-ground capacitance and not the line-to-line capacitance. This is negligible for wide, isolated lines but it becomes significant for line spacings under 3 μm [Sin82]. For feature sizes of less than 1.5 μm, the line-to-line capacitance begins to affect the total capacitance significantly, and at around 0.5 μm, it dominates and causes the total capacitance to increase sharply with further decreases in feature size, as shown in Figure 2.1 [Jen94]. The device delay, in contrast, decreases with decreasing feature size. Figure 2.2 [Jen94] shows that for feature sizes above 1 μm, nearly all the total delay is due to device delay. As feature sizes are scaled to 0.5 μm and smaller dimensions, the interconnect delay accounts for an increasing portion of the total delay, increasing from 20% at 0.5 μm to approximately 50% at 0.25 μm. This implies that a large part of the gains in speed as a result of smaller device sizes will be lost unless interconnect delay can be reduced.

Methods of Reducing Interconnect Delay

From equation 2.1, a reduction in ρ, ε_{ox} or L, or an increase in d or t_{ox} will decrease interconnect delay. Decreasing L will have an especially significant effect, because interconnect delay is proportional to the square of L. Other techniques include utilizing low resistivity metals such as copper [Ste97] and low dielectric constant ILDs such as Spin On Glasses (SOGs), polyimides and parylenes [Tin94]. MLM is another technique which has become the most prevalent in the semiconductor industry.

Multilevel Metallization

In MLM schemes, the metal interconnections span several planes and are isolated by insulating dielectric layers and are interconnected by wiring (vias) in the third dimension through holes in the dielectric planes [Mur93]. A cross-section of a MLM scheme is shown in Figure 2.3 [Sti97]. This configuration reduces interconnect delay by several means. Firstly, by having a larger number of metal levels, the packing density of metal lines need not match the packing density of the gate levels, so that the interconnect dimensions need not shrink as fast as the gate level dimensions. In addition, MLM reduces the length of the interconnections by allowing more direct routing of metal lines to take place. Finally, where long metal lines are unavoidable, these lines can be routed at the upper levels, which maintain even wider dimensions to lessen delay times on the long lines [Ste97].

The processes involved in MLM are deposition, lithography, etching and planarization. The sequence is usually as follows: (1) planarization to flatten the dielectric surface, (2) etching high aspect ratio via holes in the dielectric, and sometimes (in dual damascene technology) etching the metal lines into the dielectric as well, (3) filling the via holes with metal, (4) removing metal from regions other than the vias, (5) depositing and patterning the metal lines (6) depositing the next level of dielectric, and (7) planarization of the dielectric, if required. These process steps are repeated for different metal levels.

Planarization

Planarization requirements

With an increasing number of metal layers and shrinkage in interconnection dimensions, surface planarity has become more and more critical. Wafer surfaces can be categorized into three degrees of planarity, as illustrated in Figure 2.4: (1) Surface smoothing, where feature corners are smoothed and high aspect ratio holes are filled; (2) local planarity where surfaces are locally flat but the surface height varies across the die; and (3) global planarity where the surface is flat across the entire stepper field [Ols93].

Surface smoothing and local planarity are important for ensuring proper metal step coverage. However, with additional metal levels being added, global planarization is required, because non-planarity on the surface becomes cumulative, and severe topography can develop even with surface smoothing. This results in poor step coverage and electromigration [Ols93]. In addition, as circuit dimensions are shrunk below the sub-0.5 µm regime, lithography tools require high numerical aperture lenses to print these fine line dimensions. These lenses have a depth of field of approximately 270 nm across a 27 by 27 mm stepper field. Due to this finite depth of field and equipment tolerances , the optical steppers require a topographic variation of less than 150 nm across the stepper field. Topography can also cause photoresist thickness variations, which can cause overexposure in areas of thinner resist. In addition, variation in thickness of dielectric across the wafer will require the etching of vias of different depths, which will introduce more variability and reduce process yield. A planarized dielectric film will result in vias of the same depth in all metal levels. Finally, with multiple metal layers, even surface smoothing (explained in the next section) will lead at a cumulative increase in topography towards the final metal level, further reducing process yield [Mur93], [Ste97].

All the above factors clearly illustrate the need for global planarization in present day semiconductor manufacturing technology.

Planarization Techniques

Three main techniques used for achieving planarization are the following;

1) Bias-Sputtering: The substrate is biased so that back-sputtering occurs on the surface. Thus, sputter deposition and back-sputter etching occur simultaneously. This is an asymmetric process, and is favored at sharp corners and edges so that it can result in good step coverage. However,

deposition rates are low and ion damage takes place during the process. In addition, it does not provide large area planarization [Mur93].

2) Dry Etching (RIE) etch-back: After the CVD oxide layer has been deposited, a thick layer of photoresist or Spin On Glass (SOG) is then deposited, which covers all steps and gives a flat surface. Then a plasma or reactive ion etch process is carried out, which etches the resist and the underlying oxide at the same rate. The etching is carried out till the resist and some of the CVD oxide is etched off, leaving the surface flat. However, the process is lengthy and time consuming and often has to be repeated several times [Mur93], [Ste97].

3) Chemical Mechanical Polishing (CMP): This process, which has been briefly described earlier, has emerged as the clear choice for achieving global planarization. It is very versatile, simple and can be applied to all types of materials, from insulating dielectrics to metals.

So far, CMP has been used to planarize dielectrics and metals of several types, e.g. SiO_2, polymers, tungsten, copper, and aluminum.

Advantages of CMP

The chief advantage of CMP is that it results in global planarity. In addition, there are cost advantages. Several planarization techniques are carried out in many complex steps, which increase both cost and defect densities. CMP, on the other hand, involves only one step and often leads to a reduction or elimination of some defects. Defects such as metal stringers, poor step coverage and film particles from earlier steps are significantly reduced as a result of CMP [Lan92]. In addition, CMP is also replacing dry etch processes for metals, because of its superior removal uniformity, and also because dry etching for new interconnect materials like copper is not feasible.

Disadvantages of CMP

Because CMP is a new process, there are several parameters that need to be optimized. This means that the process windows are often narrow. In addition, several new types of defects can arise as a result of CMP. Scratching from abrasive particles, stress cracking of films, residual slurry particles, corrosive attack of slurry chemicals on wafers and equipment and film delamination are possible defects that need to be minimized to ensure a viable process [Lan92]. A particularly significant problem associated with CMP is dishing and erosion of patterned structures. This is especially severe where there is either a large difference in the properties of the two materials being polished at the final stages of the process (Copper CMP), or where extremely tight dimensional control is required (Shallow Trench Isolation (STI) which is carried out at the device level, and is explained in the section on SiO_2 CMP).These two phenomena are illustrated schematically in Figure 2.5. Dishing occurs when there are wide and isolated features being exposed towards the end of the polishing process. If the polishing slurry possesses a high selectivity, i.e. it polishes the material in the trench much faster than the surrounding material, then the polishing pad can reach into the recess and remove significant amounts of material. This dishing can degrade isolation properties of STI structures, and lead to poor electrical contacts in the case of MLM structures. Erosion occurs in areas of high pattern density, when the dielectric surrounding the metal features is polished along with the metal. This leads to a thinning of the dielectric layer along with the metal, reducing the amount of metal and dielectric, leading to increased topography and degradation of properties. Finally, because CMP is a new process, an entire new set of process and metrology tools is required to integrate it into the IC manufacturing process.

Chemical and Mechanical Effects in CMP

CMP involves chemical reactions between the slurry and the surface to be polished. In order for the reactions to continue, the reaction (and abrasion) products must be transported away from the wafer surface, and fresh reactants must be supplied. In these kinds of processes, boundary layers play a critical role. The three layers that play the most critical role in CMP are (1) the fluid boundary layer, which is the region near the wafer surface where the fluid velocity differs from the maximum; (2) the electrical double layer, which forms due to the charge associated with the wafer, particles and pad surfaces; and (3) surface films that form as a result of chemical modification of the wafer surface by the reagents present in the slurry [Ste97].

Mechanical Abrasion

In addition to physical removal of the surface layer on the wafer, one important contribution of mechanical abrasion is to break up the above mentioned boundary layers and help in transportation of reactants and products to and from the wafer surface. As a result, abrasion enhances the chemical component of CMP, along with providing the mechanical component.

Abrasion can be classified into two modes, polishing and grinding. The chief difference between the two processes is the abrasive size employed. In grinding, abrasive sizes (diameters) in the range of 1-100 μm are normally used, whereas polishing utilizes submicron (0.01-0.3 µm) size abrasives. Grinding can also be subdivided into two categories, brittle grinding and ductile grinding. Ductile grinding occurs with abrasive sizes on the lower end of the range (0.75-3.0 µm). Material removal is the result of crack initiation, and the abraded material is of the order of nanometers in size. Additionally, the surface being abraded experiences plastic flow and densification [Gol91]. This induces a compressive stress in the film, which may be beneficial in metal films, because compressive stress inhibits the harmful phenomena of stress migration and electromigration [Mur93]. Brittle grinding, on the other hand, involves crack propagation and brittle fracture, and the abraded material is of the order of microns in size. This often results in high removal rates, but the surface quality obtained is poor, and subsurface damage also takes place [Gol91].

In polishing, material removal takes place by severing of bonds on the atomic or molecular scale. The material removed is also on the order of clusters of atoms and molecules [Coo92]. Polishing can occur by either Hertzian indentation or fluid-based wear. During Hertzian indentation, the abrasive particles get dragged across the wafer and remove material from the surface. The volume of indentation depends on several factors, such as particle size, solids loading and the properties of the wafer surface. In fluid-based wear, the particles impinge on the surface and as a result, energy transfer to the wafer surface takes place, resulting in bond weakening, strain and removal of material [Coo92]. Which mechanism is responsible for material removal will depend on the nature of the fluid layer between the polishing pad and the wafer [Run94]. If the fluid layer is not continuous, then Hertzian indentation is expected to dominate, as a result of the pad dragging the particles across the wafer surface. In case of a continuous fluid layer, collisions between the abrasive particles and between the particles and the pad will accelerate them, causing them to impinge on the wafer surface with high velocities, resulting in fluid-based wear.

Effect of Particle Size

The size and concentration of abrasive particles is polishing slurries are important parameters in determining polish rate and surface quality of the polished surface. The effect of these two parameters has not been systematically characterized so far. Different researchers have obtained different (and often contradictory) conclusions as to the effect of particle size on polishing. Jairath et al. [Jai94] observed that SiO_2 polish rate increased with both particle size and concentration. Xie and Bhushan [Xie96] obtained similar results for particle size in polishing of copper and ferrite with diamond and alumina abrasives. However, Cook [Coo90] and Sivaram [Siv92] proposed that polish rate is independent of abrasive size, and Izumitani [Izu79] observed that decreased abrasive size led to higher polish rates for optical glasses. None of these studies involved a systematic variation of both particle size and concentration, making their results somewhat inconclusive. Recent studies conducted at the University of Florida [Bie98] on particle size and concentration effects in Tungsten CMP have shown that polish rate increases as particle size is reduced.

The variation of removal rate with particle size has been explained by two hypotheses. The first one states that larger particles penetrate the substrate to a greater depth, and thus should remove more material. The second hypothesis states that smaller particles are present in larger numbers in a slurry, for a given volumetric concentration. Due to this larger number of "cutting tools," smaller particles should remove material faster, although each particle may remove less material by itself. However, it must be borne in mind that particle concentration is a critical factor in determining the removal efficiency of a single particle. Some results on the effect of particle size in SiO_2 CMP will be presented in Chapter 4.

Theories of Removal Rate

The most frequently used expression for polish rate is the Preston Equation [Pre27], which was arrived at empirically by Preston, and later developed analytically by Brown et al. [Bro81].The equation states:

$$\text{Re movalRate} = \frac{\Delta H}{\Delta t} = K_p \cdot P \cdot V \qquad (2.2)$$

where ΔH is the change in height of the surface, Δt is the time of polishing, P is the pressure and V is the linear velocity of the pad with respect to the substrate being polished. K_p is the Preston coefficient, which is a process-dependent constant, which includes parameters like slurry properties, pad properties and the properties of the material being polished. Brown et al. [Bro81] derived an expression for the Preston coefficient, based only on the mechanical properties of the material being polished. Based on Hertzian indentation mechanics, they derived an expression for the elastic penetration depth of an abrasive particle as

$$\delta = \frac{3}{4} \cdot \phi \cdot \left(\frac{P}{2 \cdot K \cdot E}\right)^{2/3} \qquad (2.3)$$

where δ is the penetration depth, ϕ is the diameter of the particle, P is the applied pressure, E is the elastic modulus of the material being polished and K is the packing fraction of the particles on the surface (K=1 for a fully hexagonal close packed arrangement). Based on this equation, and assuming that the spherical particle moves along the surface at a velocity V removing a volume of material of dimensions proportional to the penetration depth, they expressed the rate of material removal as

$$\text{Rate} = \frac{\Delta H}{\Delta t} = \frac{1}{2E} \cdot P \cdot V \tag{2.4}$$

This expression is equivalent to the Preston equation, as expressed in equation 2.2, but the Preston coefficient is expressed as the inverse of twice the Young's Modulus of the material being polished. However, this coefficient still does not account for factors such as slurry and pad properties.

Polishing Pad

The polishing pad is one of the most important constituents of the CMP system, but is also one of the least understood ones. Pad structure and material properties are important in determining polish rate and planarization ability of a CMP process. Still, direct correlations between pad properties and polish performance have not been established.

In addition, conditioning is required to maintain performance over the life of the pad [Ste97]. In general, pads are composed of either a matrix of cast polyurethane foam with filler material to control hardness or polyurethane impregnated felts. Polyurethane is used because urethane chemistry allows the pad characteristics to be tailored to meet specific materials properties needs [Jai94]. The chief properties pad that are of interest are:

(1) Hardness and compressibility: The harder and more incompressible the pad, the less it will bend and conform to the wafer surface to remove material in the lower regions. Such pads have been shown to planarize more effectively. However, some global flexibility is also required to minimize possible breakage of the wafers during polishing. This has led to the use of stacked structures, consisting of a hard pad on the top and a soft one as the base (e.g. IC 1000 (hard) stacked on Suba IV (soft)).

(2) Surface morphology: This includes the microporosities that are inherent in the urethane structure, as well as the macroscopic structures (perforations, grooves) deliberately introduced on the surface to facilitate slurry transport. The surface roughness has also been shown to affect removal rate and planarity, as it determines the contact area between the pad and wafer surface.

As described earlier, surface roughness and porosity determine slurry transport to and material transport away from the wafer surface. During polishing, the pad surface can undergo plastic deformation and become smoother. This is known as glazing. Figure 2.6 shows a micrograph of a new and glazed pad. Besides glazing, the pores on the pad surface can fill up with slurry, which then clogs them up and prevents proper transport. The dried slurry in the pad pores can also release large agglomerates on to the pad surface, which can then cause scratching and surface damage. Because of these reasons, conditioning techniques are often employed to maintain the roughness and porosity of the pad surface. Typically, grids or discs coated with diamond particles are used as conditioners [Ach96]. Most commercial polishers include an arm with one of these discs attached for dedicated pad conditioning. Conditioning can be performed in-situ during polishing or between polishing runs. However, care must be taken to ensure that the conditioners do not release particles on to the pad surface [Ste97].

Chemical Effects in Metal CMP

Since CMP involves both chemical reactions and mechanical abrasion, a brief description of metal is presented, with emphasis on the chemical aspects of material removal. Since

SiO_2 CMP is the focus of this study, it will be described in detail in the next section.

Metal CMP is carried out with the purpose of removing the deposited metal from all surfaces except the lines/plugs, which are recessed into the underlying dielectric. This configuration is ideally suited for a process like CMP, which can be tailored to remove material preferentially from high spots. In metal CMP, this is achieved by adjusting the slurry chemistry to form a passive film (usually an oxide) on the metal surface by adding oxidizers or corrosion inhibitors. This passive film prevents further oxidation or dissolution of metal from recessed areas. However, the overlying (high) features come in intimate contact with the abrasives in the slurry and with the polishing pad, which causes mechanical removal of the surface film. This exposes a fresh metal surface to the slurry chemicals, resulting in formation of a new surface film, which is then removed by the abrasive particles. This sequential formation and removal of a surface passive film is desired to obtain controlled removal, and to obtain a smooth, scratch-free surface (since only the surface oxide is removed, there should be no scratches on the metal surface). The metals on which CMP is primarily carried out are Tungsten, Copper and Aluminum, although lately there has been some work on CMP of Tantalum [Har00] and other metals, which have applications as adhesion promoters and diffusion barriers.

Tungsten CMP

Tungsten has several properties which lead to its being used in metallization. These are its low thermal expansion coefficient, fairly low resistivity, high melting point and good electromigration resistance. In addition, reactive ion etching (RIE) of tungsten can be easily carried out. Finally, Chemical Vapor Deposition (CVD) of tungsten allows the deposition of a conformal coating without keyholes or gaps. As a result, tungsten films are widely used in IC manufacturing as gate contacts and vias in multilevel interconnects. For the latter application, a blanket film of tungsten is deposited on a thin adhesion layer of titanium and/or titanium nitride to fill contact holes and vias, which have been etched into a planarized (by CMP)dielectric film. Following the deposition, CMP is carried out on the tungsten surface so that the metal only remains in the vias, and is removed from everywhere else. Tungsten CMP is the most widely used metal CMP process in semiconductor manufacturing.

Tungsten CMP is typically carried out in acidic solutions in the presence of an oxidizer such as hydrogen peroxide, potassium ferricyanide, potassium iodate or ferric nitrate. According to the potential-pH equilibrium diagram for the tungsten-water system, the tungsten surface becomes passivated at pHs below 4 [Pou74]. However, in the presence of an oxidizing agent, the range of pHs in which tungsten gets passivated is extended [San75]. Polishing experiments conducted under alkaline conditions resulted in isotropic removal of tungsten, which is characteristic of a wet etching process. This is unsuitable for achieving planarization, especially during the final stages of polishing, because it can lead to the formation of recessed plugs, dishing and poor electrical connections.

The currently accepted model for tungsten CMP is the one proposed by Kaufman et al. [Kau91]. According to them, a passivating oxide is continuously formed on the metal surface in the presence of oxidizers like potassium ferricyanide ($K_3Fe(CN)_6$)and is mechanically removed by the action of the abrasive particles. The redox reaction proposed by them was as follows:

$$W + 6Fe(CN)_6^{3-} \Leftrightarrow WO_3 + 6Fe(CN)_6^{3-} + 6H^+ \qquad (2.5)$$

This surface oxide is passivating, i.e. It forms a protective film on the metal surface and prevents further oxidation and dissolution. However, when this film is broken, there is competition between the passivation and dissolution reactions. The dissolution reaction is as follows:

$$W + 6Fe(CN)_6^{3-} + 4H_2O \Leftrightarrow WO_4^{2-} + 6Fe(CN)_6^{4-} + 8H^+ \qquad (2.6)$$

This reaction is thermodynamically favored at higher pH,and is slower than the passivation reaction at lower pH, which is why Tungsten CMP is carried out under acidic conditions. Kaufman et al., however, did not present any evidence to prove that there was a tungsten oxide layer on the metal surface during CMP. However, subsequent research by Farkas et al. [Far95] showed that mechanical abrasion of tungsten metal does not contribute significantly to the CMP process, and that tungsten dissolution is not necessarily the dominant chemical reaction during CMP. In addition, Auger Electron Spectroscopy, wet etch and AC impedance measurements showed evidence of surface passivation under certain conditions. Other researchers like Kneer et al. {Kne97]conducted atomic force microscopy scans of polished tungsten films, and concluded that corrosion assisted fracture may be an important component of the removal process. In addition, Stein et al.[Ste98] compared electrochemical measurements to polishing rates measured in-situ in their electrochemical cell. They concluded that passive film formation is not necessary for tungsten CMP to take place. According to some recent results obtained by Stein et al. [Ste99a], [Ste99b], [Ste99c], polish rates in chemically identical slurries are dependent upon colloid species, and that the process temperature rise during CMP is primarily due to friction between the abrasives and tungsten surface. In addition, Atomic Force Microscopy (AFM) measurements also show that transgranular fracture or abrasion of the metal are not likely removal mechanisms during CMP. However, these results are mostly empirical, and do not have a strong enough analytical explanation.

Recent work conducted at the University of Florida [Bie98],[Bie99b], on the effect of particle size in tungsten CMP has shown that smaller particles show higher removal rates, and that surface roughness of the polished samples is essentially independent of particle size. Tribocorrosion experiments showed that surface passivation is required to obtain significant removal of tungsten. This indicates that surface oxidation kinetics play an important role in determining tungsten polishing rates, as smaller particles, with a higher abrasion frequency, polish much faster than larger particles.

In spite of all these studies, there is still a lot of work that remains to be done to conclusively establish the exact mechanism of material removal during tungsten CMP.

Aluminum CMP

As has been explained earlier, so far aluminum (Al) has been the metal of choice for metallization. Even with the advent of copper interconnects, Al still remains popular, and work is being done to integrate it in new damascene schemes. The chief advantages of Al are its low resistivity and its ability to reduce SiO_2. This leads to low contact resistance and stronger bonding. In addition, conformal Al films can be deposited using new techniques such as reflow sputtering [Kit95].However, its low melting point makes Al susceptible to electromigration problems, and limits the temperature range of subsequent processing steps. Additionally, annealing of the metal after deposition can cause silicon dissolution. These problems can be reduced by adding a small amount (around 1.0 wt.%) of silicon to the Al during deposition. In addition, addition of copper to Al increases electromigration resistance. The reason for this is expected to be due to an enhancement in the self-diffusion energy of Al, in addition to modifying the grain structure of the films [Mur93].

Lately, significant work has been carried out on CMP of Al. Wang et al. [Wan97] carried out CMP of Al and Al alloys using alumina abrasives and hydrogen peroxide (H_2O_2) as an oxidizer, in a pH range from 1.5 to 5.0. They saw that the polish rate decreased with increasing pH. In addition, they showed that the removal rate for Al alloys increased with increasing Cu concentration, due to the increased susceptibility of these films to corrosion. In addition, films deposited at a lower temperature showed higher removal rates, due to their smaller grain size (larger grain boundary area) and decreased corrosion resistance. Based on their results as a function of oxidizer concentration and slurry pH, they proposed that the chemical reactions occurring during Al CMP are as follows:

$$Al_2O_3 + 6H^+ \Leftrightarrow 2Al^{3+} + H_2O \tag{2.7}$$

Hydrogen peroxide dissociates as follows:

$$H_2O_2 \Leftrightarrow HO_2^- + H^+ \tag{2.8}$$

The exposed Al can be re-oxidized as follows:

$$2Al + 3HO_2^- + 3H^+ \Leftrightarrow Al_2O_3 + 3H_2O \tag{2.9}$$

An optimum removal rate will be obtained when the two reactions counterbalance each other. This hypothesis assumes that Al_2O_3 on the metal surface is too hard to be effectively removed. This assumption has not yet been verified.

Kallingal et al. [Kal98] conducted Al CMP experiments and electrochemical measurements using potassium dichromate as an oxidizer. They obtained low polish rates and severe scratching while polishing with abrasives and oxidizer. However, on addition of 5 vol.% acid solution (70%

phosphoric acid, 20% sulfuric acid and 10% nitric acid), a higher polish rate and reduced scratching was obtained. The explanation for their results was rather sketchy.

Recently, Wrschka et al. [Wrs99] reported results from X-ray Photoelectron Spectroscopy (XPS) measurements carried out on Al samples polished using alumina particles and H_2O_2 oxidizer. They saw a correlation between thickness of Al_2O_3 on the polished samples and removal rate, with lower oxide thickness corresponding to a higher removal rate. This seems to indicate that removal is occurring by removal of the oxide that forms on the metal surface in the presence of the oxidizer. They also developed an empirical model to explain pressure and velocity effects in their experiments. However, the exact nature of the chemical component in Al CMP is still not certain.

Very recently, Kuo and Tsai [Kuo00] characterized the electrochemical behavior of Al in a CMP slurry using potentiodynamic polarization and impedance spectroscopy. The slurry was composed of alumina particles, phosphoric acid and citric acid. Tests conducted during polishing showed that corrosion potential decreased and dissolution rate (using corrosion current as an indicator) increased with increasing contact pressure and platen rotation speed. Surface analysis using XPS indicated the presence of Al_2O_3,

$Al(OH)_3$ and $AlPO_4$ on the metal surface, which comprised the passive film.

Although the newer studies seem to be shedding more light on the mechanisms of Al CMP, more work is clearly required, especially for characterizing abrasive effects in the process.

Copper CMP

With the advent of submicron technology in IC manufacturing, need for a high conductivity metal, for applications as interconnections both on and off the chip, has brought attention to Copper (Cu). Copper interconnects have several advantages over conventional W/Al technology. Firstly, Copper has a much lower resistivity than W and Al; 1.67 μΩ-cm for Cu versus 2.66 μΩ-cm for Al and 5.65 μΩ-cm for W. This means that higher operating speeds can be attained. Secondly, due to its higher melting point, it possesses a much higher electromigration resistance than Al, enabling it to be used for fabricating fine metal lines. This also enables it to replace W in the high aspect-ratio vias, thus eliminating the necessity for using two different metals.

However, in spite of these advantages, several challenges are involved in integrating Cu into IC fabrication processes. Firstly, Copper diffuses very rapidly through SiO_2, and forms deep levels in Silicon, which degrade the electrical performance of the devices in the chip. Cu impurities in the dielectric also lead to significant leakage currents. Secondly, its adhesion to SiO_2 is very poor. Finally, because volatile Cu compounds form only at elevated temperatures, Reactive Ion Etching (RIE) processes are impracticable. The first two issues are dealt with by depositing a diffusion barrier/adhesion promoter before depositing the Cu. This is usually Tantalum or Tantalum Nitride. Tantalum is an attractive barrier metal because of its high melting point and its immiscibility with Copper. It is also highly reactive and forms strong metal-metal bonds, much like Titanium does for Aluminum interconnects. Thus, it should provide a low-resistance ohmic contact with good adhesion to copper. Doping the Ta film with Nitrogen blocks grain boundary diffusion pathways. As a consequence, nitrided Ta (TaN), formed by reactive sputtering of Ta in a nitrogen ambient, is also an attractive barrier material. One specific advantage of PVD Ta is its excellent step coverage, which can be further extended by ionized PVD processes. Alternative materials under consideration, especially for future processes, include Tungsten Nitride and Titanium Silicon Nitride [Jac98]. The lack of dry etching processes is overcome by using the "damascene" process. In this process, the vias and trenches are both etched into the dielectric, following which the metal is deposited. CMP of the metal is then carried out, leaving only the recessed metal in the dielectric. The advantages of this process are that etching is not required, and also that the Cu can be deposited in a single step (dual damascene), and also that the final surface after CMP is planarized. This means that the subsequently deposited dielectric will also be planar, and thus will not have to undergo CMP. As a result, the number of process steps is reduced. The single and dual damascene process steps are schematically shown in Figure 2.7.

Electroplating has become the process of choice for depositing the Cu films. This process has several advantages compared to PVD and CVD due to its low cost, low process temperature (reduces copper diffusion in dielectric) and good ability to fill the high aspect ratio vias in present day and future interconnects. The chief disadvantage associated with this process is that it requires deposition of a thin seed layer prior to the deposition step. This seed layer is usually deposited by PVD or CVD. Following the seed layer deposition, Cu is electroplated on the wafer surface [Jac98]. However, electroplated Cu films tend to recrystallize at room temperature. The as-plated films have an equiaxed, fine-grained and uniform structure (around 0.1 mm grains size in a 1.0 mm thick film). Over a period of hours to days at room temperature, the small-grained Cu undergoes secondary recrystallization to a final grain size of several microns [Gro99]. Because of this, all plated films are annealed prior to further processing, in order to obtain a uniform grain size distribution. After the annealing, CMP is carried out to remove the Cu and barrier layer from the field areas. Because of the large difference in the mechanical properties of Cu and Ta, usually a two-step or even a three-step CMP process is required, to minimize dishing and erosion of the polished structures (Figure 2.5).

Although Cu CMP has been studied by several researchers, the mechanisms of material removal are still unclear, and the process is also not yet optimized. The basis for selecting a slurry chemistry is usually the potential-pH (Pourbaix) diagram for Cu-H_2O, according to which oxides of Cu do not form below pH 5, and that Cu dissolves as Cu^{2+} ions. For the pH range of 7-13, Cu_2O formation is more likely at lower potentials, while CuO forms at higher potentials. Beyond pH 13, CuO_2^{2-} can form. Some earlier studies on Cu CMP used HNO_3 as an oxidizer in polishing experiments and electrochemical measurements.

Although high removal rates were obtained, using Al_2O_3 as the abrasive (Al_2O_3 was used in the subsequent studies described here as well) severe scratching was observed. In addition, Cu dissolution (etch) rates were undesirably high. This was overcome by the addition of Benzotriazole (BTA), which functions as a corrosion inhibitor by forming a protective film on the Cu surface [Car95]. Studies by Wang et al. [Wan97b] on the effect of BTA on Cu corrosion show that addition of a small (0.01M) amount effectively passivated the Cu surface. This passive film also resulted in a reduced removal rate. The authors also showed that adding a very small amount (3 vol.%) of oxidizer (H_2O_2) resulted in a sudden increase in the corrosion rate. However, addition of larger amounts actually decreased the corrosion of the Cu, indicating the formation of a passivating oxide film on the surface at higher oxidizer concentrations. Recent studies (unpublished) have confirmed these observations.

NH_4OH based chemistries showed formation of a relatively passive film, due to their higher pH. This makes them superior for planarization purposes. Additionally, the NH_4^+ ions are effective complexing agents for Cu ions in solution. This is accomplished by their ability to shield their ionic charge, allowing closer spacing in solution and thus higher solubility. As a result, the abraded Cu particle could also be dissolved and removed from the vicinity of the wafer surface. This dissolution rate is enhanced by the addition of an oxidizer such as potassium ferricyanide. Studies by Steigerwald et al. [Ste95] showed that although etch rates of Cu in ferricyanide/NH_4OH solutions were low, polish rates increased with ferricyanide concentration. Similar behavior was observed for the polishing of Cu_2O films grown on Cu, implying the removal of the abraded particles by dissolution. Luo et al. [Luo97] also conducted Cu CMP with NH_4OH based slurries. They found an increase in polish rate with the addition of 0.3 wt.% NH_4OH. No increases were observed for higher concentrations. Addition of an oxidizer ($NaClO_3$) increased the removal rate significantly. Addition of BTA reduced the Cu dissolution rate, while affecting removal rates only slightly. In-situ electrochemical measurements showed that the contribution of etching to the Cu polish rate was minimal. Recent studies at the University of Florida (unpublished) using iodate and iodine based chemistries have shown promising results.

Although these studies show that significant progress is being made in developing slurry chemistries for Cu CMP, our understanding of the process is still limited, and there is a lot of margin for process development. A very critical issue that needs to be addressed is the vast difference in polishing rates for Cu and Ta (barrier). Ta being a hard metal, polishes much slower than Cu, resulting in dishing of the Cu lines. On the other hand, using slurries that are less selective to Ta often results in loss of dielectric, leading to erosion in regions of high pattern density. Post-CMP cleaning is another big issue in this field, as abrasives often get mechanically embedded in the Cu, making them very hard to remove.

CMP of Silicon Dioxide

SiO_2 CMP has been practiced for years in the form of glass polishing for optical fabrication. Several mechanisms for glass polishing have been proposed and have been reviewed by Holland [Hol64] and Izumitani [Izu79]. They include (1) a wear mechanism (2) a flow mechanism and (3) a chemo-mechanical mechanism. According to the wear mechanism, the glass surface is mechanically removed during polishing, and as a result the surface is made smooth, because the high points on the surface are preferentially worn down as compared to the low points. The flow mechanism states that the glass flows during polishing, which results in the material at the peaks flowing into the valleys (low features) till the surface becomes smooth. The chemical mechanism states that surface dissolution is accelerated by the pressure imposed by the abrasive particles, resulting in material removal. Since the high areas experience higher pressures, they dissolve faster, leading to surface smoothening. Izumitani [Izu79] studied the correlation between surface hardness, softening point and chemical resistance (durability) of several silicate and borate glasses, in order to determine which of the aforementioned mechanisms dominates. Figure 2.8 (a-c) shows polishing rates of those glasses as a function of hardness (determined by Vickers microindentation), softening temperature (defined as the deformation temperature of the expansion curve) and chemical durability (determined by measuring the weight loss of the glasses in water). The only factor correlating to polishing rate is chemical durability, suggesting that there is indeed a strong chemical component in glass polishing [Izu79]. Izumitani also conducted polishing experiments in oil and under dry conditions. In both cases (as shown in Figure 2.9) the polishing rate was proportional to the hardness of the glasses, and was significantly lower than the polishing rate under aqueous conditions. This suggested that dry polishing and oil polishing are purely mechanical processes, and that there is a strong chemical component to glass polishing in water, which is responsible for the enhanced removal rate.

Role of water in glass (SiO_2) polishing

The above studies have shown the importance of water to the CMP process. Silica has been known to chemically interact with and dissolve in water. Water can penetrate a SiO_2 surface either by diffusing in through void spaces between oxygens in the structure as an intact molecular species or it can undergo hydrolysis and condensation reactions with Si-O bonds as follows:

$$H_2O + Si - O - Si \Leftrightarrow 2Si - OH \tag{2.10}$$

Since SiO_2 structures do not contain openings which are large enough to admit molecular water, reversible hydrolysis reactions are the most significant factors in determining dissolution behavior. The tetrahedral SiO_4 sites in glass are susceptible to attack by OH^- to form a reactive five-coordinated intermediate which can decompose to rupture the Si-O-Si bond [Bun94].

$$\begin{aligned} & Si - O - Si - (OH)_3 + OH^- \rightarrow Si - O - Si - (OH)_4 \\ & \rightarrow Si - O^- + Si - (OH)_4 \end{aligned} \tag{2.11}$$

From the above reaction, it can be seen that the rate of hydrolysis leading to dissolution will increase if the pH (i.e. the OH- concentration) increases. In addition, the silicic acid $Si(OH)_4$ also forms more soluble species at high pHs [Sjo96]. As a consequence of this, solubility of silica increases exponentially at pHs higher than 10. Additionally, silica solubility is also affected by external stresses. Several studies have been carried out on the diffusion of water into glass surfaces under externally applied loads. Hirao et al. [Hir87] conducted Knoop indentation measurements on glasses in various liquids. Infrared absorbance spectra of the indentation (Figure 2.10) show that only water enters into the glass as a result of the indentation, whereas indentation under other liquids does not lead to water entry. Nogami and Tomozawa [Nog84] studied the diffusion of water in silica as a function of hydrostatic pressure and applied uniaxial stress. They observed that the diffusion coefficient of water increased exponentially with increasing tensile stress and decreased with increasing compressive stress and increasing hydrostatic pressure. The solubility of water showed an opposite trend, namely, it decreased exponentially with increasing tensile stress and increased with increasing compressive stress and hydrostatic pressure. These studies, along with other old studies on glass polishing, were used by Cook [Coo90] to propose a model to explain glass polishing. According to him, an abrasive particle acts like an indenter, and promotes water entry into the silica surface due to the pressure applied by it. As the particle moves across the surface, a stress field is generated in the glass surface, with compressive stresses in front of the particle, and tensile stresses behind it. In front of the particle, hydrostatic pressure and compressive stresses in the glass promote water entry into the glass surface, leading to dissolution of SiO_2 by breaking Si-O bonds, as described earlier. However, water diffusion into the bulk is inhibited by the compressive stress. At the trailing edge of the particle, the relief of hydrostatic pressure, combined with the tensile stress in the glass surface, leads to rapid diffusion of water into the silica. This is accompanied by a reduced solubility of the dissolution products of silica, leading to some reprecipitation on the glass surface. As a result, net material removal occurs only when the rate of dissolution is greater than the condensation rate [Coo90]. This means that the dissolved $Si(OH)_4$ should be removed from the vicinity of the surface as efficiently as possible. This process can be carried out by the motion (flow) of the slurry or by other mechanisms including (1) adsorption onto the abrasive particles and (2) precipitation of colloidal SiO_2 which is then swept away by the slurry flow.

Interaction between abrasive particles and oxide surface

Some abrasives may interact chemically with the oxide surface or the dissolution products, thereby resulting in high polish rates. For example, ceria (cerium oxide) exhibits a so-called "chemical tooth" which causes it to polish glass very rapidly. Cook [Coo90] estimated that Ceria is 5 x 10^8 times more efficient than silica at removing $Si(OH)_4$ (in terms of molecules removed per collision). This results in Ceria abrasives having a much higher polishing rate than Silica abrasives. The reason for this higher polishing rate, according to Cook, is that abrasives like Ceria and Zirconia (ZrO_2) chemically react and bond with the silica dissolution products. Additionally, salts of these compounds, when added to polishing slurries, have been known to enhance polishing rates significantly. Yakovleva [Yak74] found that polishing rates for many glasses were increased on the addition of Zirconium Sulfate to the ZrO_2 slurry. Similar increases in removal rate were reported by Silvernail [Sil82] on the addition of $Ce(OH)_4$ to polishing suspensions of CeO_2, ZrO_2 and ThO_2. $Zr(OH)_4$ and $Th(OH)_4$ showed similar effects. Interestingly, previously inactive oxides such as Y_2O_3, Tb_2O_3 and Gd_2O_3 showed higher polishing rates when $Ce(OH)_4$ was added to their suspensions. Addition of $Si(OH)_4$ showed no such effect, and in one study, reduced polish rates for CeO_2 and ZrO_2 suspensions [Kud79]. Cook also stated that in the pH range used for glass polishing (pH 7-9), CeO_2 and ZrO_2 surfaces have little to no measurable surface charge. Thus their surfaces, being amphoteric, are able to adsorb and exchange both cationic and anionic species. Similar behavior was observed for polyvalent metal ions in solution, as evidenced by their strong adsorption on the silica surface over a pH range consistent with their stability. This adsorption and the resultant amphoterism of the surface was used to explain the ability of such species to precipitate silica colloids from solution [Ile79], suppress aqueous corrosion and affect static fatigue of glass [Fox80]. This ability to precipitate colloidal silica from solution was interpreted by Cook as the basis of the activation of the polishing process when salts of the polishing compound are added to the polishing slurry. Some studies on polishing optical glasses using a wide variety of abrasives were conducted several years back [Sil82], [Kal62] and their results (shown in Figure 2.11) indicate that the variation in polish rate with the Iso-Electric Point (IEP) of the abrasive was quite pronounced. The IEP of a surface is defined as the pH at which the surface possesses no measurable charge. Maximum polish rates were obtained from abrasives having an IEP ≈7. This lent credence to Cook's hypothesis of neutral surfaces being able to adsorb dissolution and abrasion products more effectively. However, the polishing conditions such as particle size and slurry pH are not clearly specified by the authors, and Silvernail has used the same weight fraction of different oxides instead of the same volume fraction, thus raising questions as to the validity of their results. Based on these studies, Cook hypothesized that the following chemical steps occur during SiO_2 (or glass) polishing:

(1) Reaction of the surface $Si-O^-$ groups on the glass surface with M-OH groups on the particle surface occurs, forming a M-O-Si bond.

(2) As the particle moves away from the bonding site, the M-O-Si bond is strained, leading to either a rupture of the M-O bond or the Si-O bond, depending on the relative bond strengths. If the M-O bond is stronger, the silica bonds with the particle surface and is removed from the substrate region. However, even otherwise, the strain is not expected to be sufficient to cause the breakage of multiple Si-O linkages, but for a Si-O species having only one linkage to the network, the elastic recoil and strain energy released by the bond rupture can promote scission of the last bridging oxygen atom of the network, releasing a positively charged intermediate species into solution.

(3) The adjacent molecular water and hydroxyls react with the particle surface and the silica intermediate to reform M-OH on the particle surface and a free silicic acid molecule.

(4) The silicic acid molecule can then either redeposit on the glass surface, or can complex with adjacent metal ion sites on the particle surface.

This hypothesis was supported by a roughly linear fit that Cook was able to obtain for the results of Kaller [Kal62] and Silvernail [Sil82] for polishing rate as a function of the inverse logarithm of the product of the oxide (particle) M-O bond strength and the absolute value of the difference of the IEP from the slurry pH. Cook's assumptions of slurry pH is not clearly stated, however.

This summary of glass polishing studies shows that although significant work has been done, the mechanics and chemistry of the process is still not fully understood, especially the interactions of the abrasives with the glass surface during polishing.

SiO_2 CMP in microelectronics manufacturing

As explained earlier, the widespread adoption of MLM technologies has necessitated the adoption of planarization techniques, and CMP has emerged as the process of choice.

SiO_2 is the dielectric of choice for insulating the different metal levels, and a flat surface is important for ensuring repeatable and reliable interconnect performance. Typically, the SiO_2 is deposited by CVD to obtain high deposition rates and good gap filling. Sometimes doped SiO_2 is also used, the most common examples being phosphosilicate glasses (PSG) and Borophosphosilicate glasses (BPSG). The Boron reduces the viscosity of the films, reducing their reflow temperature, while the Phosphorus provides trapping sites for alkali metals [Wol86].

Another application of SiO_2 CMP is in the area of Shallow Trench Isolation (STI) at the device level. For a long time, local oxidation of silicon (LOCOS) was used to electrically isolate devices in integrated circuits. With smaller geometries and higher circuit densities being adopted, the requirements for isolation have become more stringent, and problems such as poor planarity, lateral encroachment of the oxide into active regions began to arise. As a consequence, an alternative process called Shallow Trench Isolation (STI) was adopted, which is preferred for device geometries smaller than 0.35 µm. The process involves etching a trench pattern through a nitride layer, a thin pad oxide layer, and into the silicon. Subsequently, SiO_2 is deposited by CVD over the entire wafer, filling the trench area and overlying the nitride region. CMP is then carried out to remove the oxide from everywhere except the trench region. The remaining nitride is then removed by a wet phosphoric acid clean or by reactive ion etching [Yu 92],[Lin 99]. A schematic illustration of this process is shown in Figure 2.12. The STI CMP process also suffers from problems like dishing of the isolation oxides and erosion of the nitride over the active regions. Since this process is carried out at the device level, good process control and low defect density are even more critical here.

SiO_2 CMP is typically carried out using a colloidal suspension of SiO_2 particles at high pH (10.5-11.0). The combination of mechanical abrasion and chemical dissolution enables high removal rates to be obtained. Lately CeO_2 slurries are also being used, especially for STI CMP, because of their good selectivity to Silicon Nitride. The details of the removal mechanism have been explained in the previous section. One of the earliest works in this regard was published by Patrick et al. [Pat91]. Other researchers have also studied this process in some detail, but most were focused on process optimization and studying the response of patterned surfaces to polishing. The mechanisms of glass polishing are accepted as being applicable to the polishing of SiO_2 thin films as well. An interesting study on the effect of film mechanical properties on polishing rates was conducted by Liu et al. [Liu95]. The mechanical properties of SiO_2 films prepared by different techniques were characterized and correlated to their CMP removal rate. Films with tensile stresses tended to have lower hardness and polish faster than those with compressive stresses. Thermal oxide films were hardest, and polished the slowest. FTIR analysis of the films showed that the Si-O bond densities of the films exhibited a linear variation with the film hardness, indicating that the more open structure of CVD films exhibits lower hardness and is more easily polished.

Liu et al. [Liu95] conducted CMP experiments on PSG and BPSG films, and showed that polish rate increased with both Phosphorus and Boron concentration, although the hardness of the films was not significantly affected. This was attributed to the faster diffusion of water through the more open glass structure. Similar results were also obtained by Fang et al. [Fan00] for CMP of PSG, where they showed a linear increase in polish rate with Phosphorus concentration.

CMP of Low Dielectric Constant Materials

The need for new interlayer dielectric (ILD) materials arises from the high dielectric constant (K) of SiO_2. Lower K values are sought to reduce the capacitive component of the RC delay in interconnects. Several materials are under consideration, including Fluorine doped SiO_2, spin-on glasses, polymers and sol-gel materials (xerogels/aerogels). The main issues with these materials are their mechanical properties, moisture intake, adhesion to the underlying layer and long-term reliability [Mur96]. Fluorine doped SiO_2 films can have a K of about 3, significantly lower than that for a pure SiO_2 film. Tseng et al. [Tse97] studied the materials properties and CMP of PECVD Fluorine doped SiO_2 films for different Fluorine concentrations. They found that polish rate increased significantly with fluorine concentration, and this was correlated to the lower hardness of these films. Additionally, increases in refractive index after polishing were observed for films containing more than 5.8 atomic % fluorine. This was interpreted as being due to the increased susceptibility of these films to chemical attack, as it was not a function of polishing pressure. This could also have led to a degradation in the low-k properties of the films.

Homma et al. [Hom97] conducted CMP experiments on organic Spin on Glasses (SOG), and found that an alkaline CeO_2 slurry provided high removal rates and good selectivity to the underlying SiO_2 film. However, the mechanism for removal was not explained. Wang et al. [Wan97c] polished alkyl siloxane films using fumed SiO_2 slurry and a ZrO_2 based slurry. The SiO_2 slurry showed decreasing removal rate with increasing organic content, while the ZrO_2 slurry showed higher removal rates. Additionally, the polish selectivity relative to SiO_2 could be adjusted using various amounts of tetra-alkyl substituted ammonium bromide (TBAH). A speculative mechanism was postulated to explain these results, based on the hydrophobic interactions between the TBAH and siloxane surface. Recently, Chen et al. [Che99] reported new results on polishing Hydrogen Silsesquioxane (HSQ) and Methyl Silsesquioxane (MSQ), which are also spin-on siloxane glasses. Two different ZrO_2 based slurries were used, one with a pH of 4.6, and the other with a pH of 10.0. Their results showed that the MSQ exhibited a lower removal rate, due to its hydrophobic surface, and that the acidic slurry polished faster than the alkaline slurry. This was explained as being due to the electrostatic attraction between the positively charged ZrO_2 particles in the acidic slurry and the negatively charged backbone of the SOGs. Higher downforce (polishing pressure) also led to higher removal rates and higher non-uniformity of the polished films.

Other organic polymers, with lower dielectric constants, have also been studied. Parylene-N, Benzocyclobutene (BCB) and Polyarylether are some of the more common examples. Yang et al. [Yan97a], [Yan97b], and Neirynck et al. [Nei96] have conducted CMP experiments on both Parylene (vapor deposited) and BCB (spun on) films, and characterized the polished films using XPS and AFM. They noticed that the higher the quality of the deposited film, the better the quality of the polished films, i.e. films with excess oxygen content showed greater structural changes after polishing. Also, addition of surfactant to the slurries increased their polish rate, presumably due to enhanced wetting of the hydrophobic polymer surface. A recent publication by Borst et al. [Bor99] on CMP of BCB and SiLK™ (from Dow Chemical), shows that the near-surface region of both polymers becomes more oxygenated after CMP. This is believed to be due to the oxidizers present in the polishing slurries. A "physically based" model to explain removal in polymer CMP was also proposed. Hara et al. [Har99] have published results showing that Polyarylether (Flare™, Allied Signal) can be polished very effectively by MnO_2 slurries, with a much better polish rate and surface finish than that obtained by fumed SiO_2 slurries. This was attributed to the higher "chemical activity" of the MnO_2

particles. However, what kind of chemical reactions were occurring during polishing was not specified.

Scope of This Dissertation

The preceding literature survey shows that although significant work has been conducted in the area of CMP, a fundamental understanding of various aspects of the process is still lacking. This thesis will focus on understanding and characterizing the SiO_2 CMP process from the particle and slurry chemistry perspective. The effect of various parameters such as particle size, concentration, density, and effect of slurry chemistry parameters like pH and ionic strength on SiO_2 CMP will be presented. Additionally, some results obtained from a novel in-situ friction force measurement apparatus, detailing the effect of various parameters such as roughness, pad conditioning and solution chemistry will be presented. The results not only shed new light on certain aspects of the process, but also indicate promising new directions for research in this area.

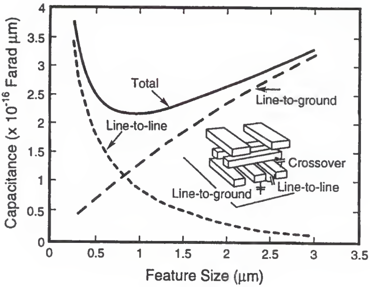

Figure 2.1: Capacitance associated with metal lines as a function of feature size [Jen94]

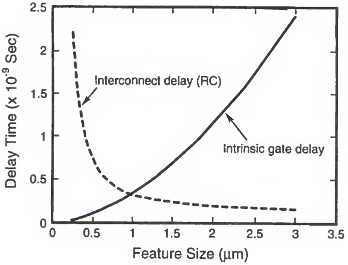

Figure 2.2: Gate delay and Interconnect delay as a function of minimum feature size [Jen94]

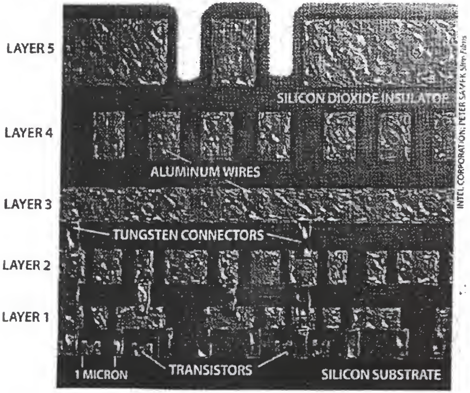

INTEL CORPORATION; PETER SAMEK Slim Films

Figure 2.3: Cross-section of Multi Level Metallization (MLM) Scheme [Sti97]

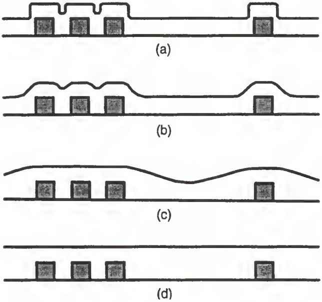

Figure 2.4: Degrees of Planarity (a) Unplanarized (b) Surface Smoothing (c) Local Planarization (d) Global Planarization [Ols93]

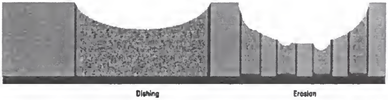

Figure 2.5: Schematic illustration of dishing and erosion [Sin00]

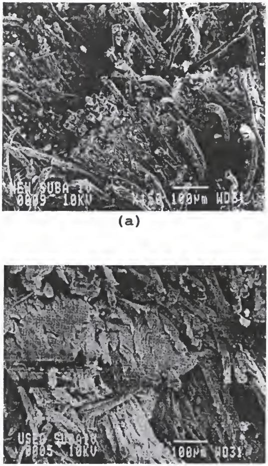

(a)

(b)

Figure 2.6: (a) New and (b) glazed Suba IV pad [Ste97]

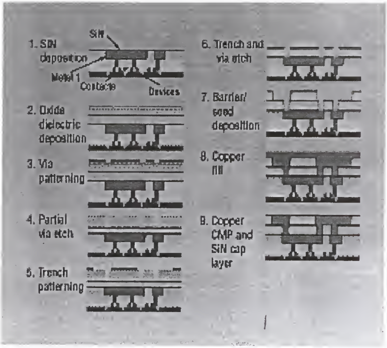

Figure 2.7: Process flow for a dual damascene Copper Interconnect Process [Jac98]

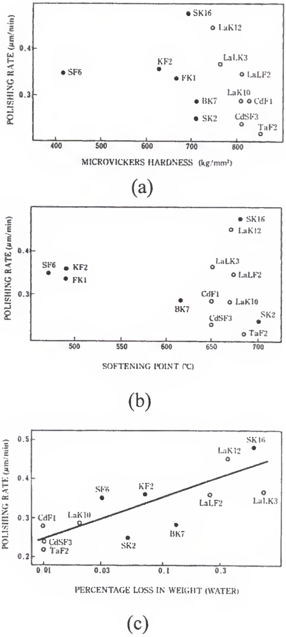

Figure 2.8: Polishing rate of various glasses as a function of (a) Vickers Microhardness (b) Softening Point and (c) Weight loss in water [Izu79]

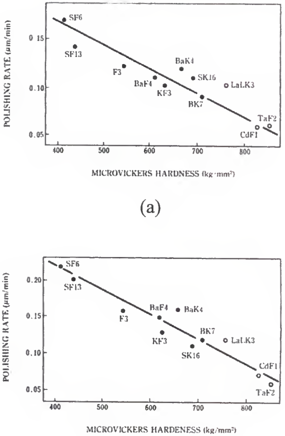

(a)

(b)

Figure 2.9: Polishing rate of various glasses as a function of Vickers Microhardness for (a) Oil Polishing (b) Dry Polishing [Izu79]

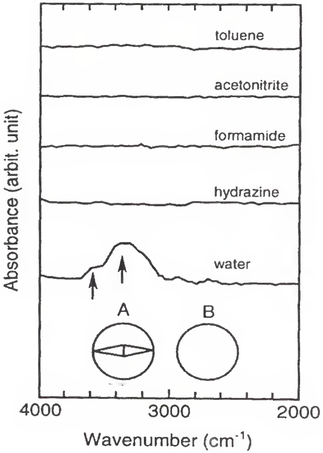

Figure 2.10: Penetration of different liquids into a glass surface during indentation [Hir87]

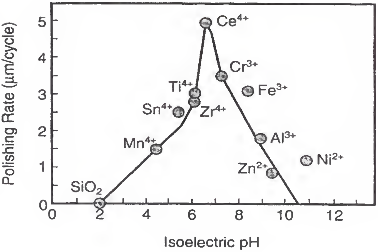

Figure 2.11: Polishing rate of various abrasives as a function of their Isoelectric Point (IEP) [Kal62], [Sil82]

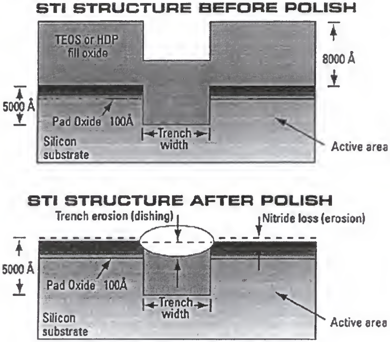

Figure 2.12: Schematic illustration of STI CMP Process [Ste97]

CHAPTER 3
IN-SITU FRICTION FORCE MEASUREMENTS

Introduction

In any process, in-situ measurements are very useful tools for on-line monitoring of process conditions. So far, the techniques used in CMP include motor torque measurements for end-point detection in metal CMP and optical interferometry for removal rates in dielectrics. Additionally, research has been done on slurry flow beneath a wafer during CMP using imaging techniques [Cop00], vertical wafer displacement from the pad surface during polishing [Mes97], and on pressure distribution at the wafer-pad interface [Tic99]. However, no in-situ technique has been developed to monitor chemical effects in a mechanically active CMP environment, detect pad degradation or to measure dynamic changes in surface roughness. In this study, a novel in-situ friction force apparatus was built, which operates in conjunction with the polishing machine. This chapter deals with the principle of the measurement, details of the instrument, and presents some of the results obtained from this study. In particular, the effect of surface roughness, solution chemistry (pH and ionic strength) and pad condition on friction forces is presented.

Materials and Methods

Setup of Instrument

A schematic illustration of the friction force system is shown in Figure 3.1. The apparatus consists of a rectangular aluminum block on which the samples are mounted. For most of these studies, a sample size of 1.5 in. X 0.5 in. was used. The block is then loaded with the desired weights and placed in a restraining fixture mounted over the polisher, which holds it in place and restricts its movement to the direction of rotation of the polisher platen. The polisher is described in detail in the next chapter. When the platen starts rotating, the frictional drag between the polishing pad and the sample causes the sample and block to move in the direction of rotation of the platen and press against a force transducer, which then records the compressive force exerted on it. A Sensotec™ Model 31 load cell is used as the force transducer. This load cell has a load range of 1000 g, and is temperature compensated from 50 to 150 F. Its output is connected to a data acquisition system, with a data sample being taken every 250 ms. The samples used for this study were as follows: (1) Chemical Vapor Deposited (CVD) SiO_2 deposited on *p*-type (100) silicon (a) As-deposited and (b) polished on a commercial CMP polisher (2) CVD Tungsten on *p*-type (100) silicon (a) as-deposited and (b) polished on a commercial CMP polisher. Rodel IC 1000/Suba IV™ stacked pads were used for all experiments, and were pre-conditioned using a Grid-Abrade™ Diamond pad conditioner before each experiment.

To improve the signal to noise ratio and to delineate the mechanical and chemical effects, particle free slurries were used in these experiments. The slurries consisted of deionized water adjusted to the desired values of pH and ionic strength. The pH was adjusted using HNO_3 and NaOH. $NaNO_3$ was used to adjust the ionic strength.

Atomic Force Microscopy (AFM)

The primary characterization technique used in this study was Atomic Force Microscopy, which was used to characterize the surface morphology and roughness of the different samples. A Digital Instruments Nanoscope III AFM was used for this purpose. AFM probes the surface of the sample with a very sharply etched silicon nitride tip (which is a couple of hundred angstroms in diameter). This tip is attached at the free end of a cantilever that is 100 to 200 µm long. Forces between the tip and the sample cause the cantilever to bend or deflect. As the tip is brought close to the sample surface, it experiences a weak attractive force, due to long-range Van der Waals interactions. This attraction increases until the atoms are so close to each other that their electron clouds begin to repel each other. This electrostatic repulsion progressively weakens the attractive force as the interatomic separation decreases. The force goes to zero when the distance between the atoms reaches a couple of angstroms. When the total Van der Waals force becomes positive (repulsive), the tip is in contact with the sample. This is called contact mode AFM. When the tip is in intermittent contact with the surface, it is called tapping mode AFM. In contact mode AFM, the deflection of the cantilever is monitored by a laser beam which bounces off the back of the cantilever onto a potition-sensitive photodetector. A feedback loop is used to maintain a constant deflection between the cantilever and the sample by moving the scanner vertically. This constant deflection ensures a constant force between the tip and the sample. The distance moved by the scanner at each point on the scan is recorded by the computer to generate the topographic profile of the sample. From this data, other information such as step heights, roughness and friction can also be obtained.

Streaming Potential measurements were also used to characterize the charge on the polishing pad surface. These measurements are used to determine surface charge on flat plates, packed beds of particles, fibers and other large surfaces. The details of the particular instrument and measurement technique are described elsewhere [Rau00].

Results and Discussion

Effect of Surface Roughness

The lateral frictional forces were monitored for silica and tungsten samples possessing different surface roughness. For this study, the pressure and platen velocity were fixed at 29.0 kPa and 150 rpm (2.19 m/s), and the ionic strength of the Deionized (DI) water solutions used was fixed at 10^{-3} M. The pH was fixed at 11.00 for the SiO_2 samples, and DI water with unadjusted pH was used for the Tungsten samples. Figure 3.2 shows the surface morphology of rough and smooth silica samples used in this experiment. The rough samples possessed a RMS surface roughness of approximately 2.65 nm, while the smooth samples had a RMS surface roughness of approximately 0.88 nm. The lateral force response measurements for each sample type are shown in Figure 3.3. After a very small initial equilibration period, the force curve showed a linear behavior, and a slightly negative slope. The figure also shows that the samples with lower surface roughness exhibited a low friction value. The relatively constant force vs. time curve for silica can be attributed to the fact that there was little change in the surface morphology of silica during the measurement.

Figure 3.4 shows the surface morphology for tungsten samples possessing different roughnesses. The rough samples possessed a RMS surface roughness of approximately 13.75 nm, while the smooth tungsten samples had a RMS roughness of approximately 1.83 nm. In contrast to the force curves for silica, the rough tungsten samples initially showed a large decrease in friction followed by a slower decrease with time, as shown in Figure 3.5. This lateral force response can be correlated with the change in surface morphology of rough tungsten films during the experiment. Figure 3.6 shows the AFM morphology of the rough tungsten films after the experiment. The figure shows that the surface morphology after the experiment is different from the as-received samples, and has a slightly lower RMS roughness (11.92 nm) and a significantly lower peak-to-valley maximum of 83 nm (as compared to 121 nm at the beginning of the experiment). In contrast to rough tungsten samples, smooth tungsten films showed a different lateral force response. After the initial equilibration period, the lateral frictional force remained constant with time. Surface morphology and roughness measurements (AFM) conducted after the experiment on the smooth tungsten films confirmed that no perceptible change in surface morphology occurred during the force measurements. Also, it can be seen that the friction forces for rough tungsten stabilize at values that are quite close to those of smooth tungsten films, although the difference in surface roughness is considerable. This indicates that the absolute values of the forces are not as significant as the change in friction with time, which indicates a change in the surface morphology of both the tungsten and the polishing pad. Hayward et al [Hay92] have obtained similar results for sliding tests conducted on CVD diamond films, where rough films showed a decrease in friction with sliding time, and polished films showed relatively constant friction values. For their experiments too, rough films subjected to sliding stabilized at friction coefficients that were quite close to those of polished (smooth) diamond films, even though the difference in roughness was considerable. The "dual sloped" nature of the force response curves is probably due to a "breaking-in" phenomenon, when there is a rapid reduction in roughness of the interacting surfaces, followed by a slower wearing down process.

The lateral force measurements clearly show the dependence of the force response curve on the surface morphology of the surface during the experiment. These results can be explained by standard theories of friction and contact between two surfaces. When two surfaces come in contact in the presence of an external load, then the friction between them can be due to localized adhesion or resistance due to interaction between the asperities on the surface [Hal75]. Typically, friction force can be expressed as :

$$F = A.s \tag{3.2}$$

where "A" is the real area of contact and "s" is the specific friction force, that is, the friction per unit area. If the chemical (slurry) conditions of the system are kept constant, then *"s"* is expected to be a constant, and the friction will be solely dependent on the area of contact between the two surfaces.

For materials which plastically deform, plastic deformation of asperities occurs in the contact region, and the real area of contact is then dependent on the applied load [Bow64], [Ili80]. For these studies, an asperity climbing mechanism seems to be dominant, similar to that proposed for friction in diamond by Tabor [Tab79]. According to the model, more energy is consumed in the sliding of rough surfaces, due to the fact that the asperities have to "climb" over each other. This shows up as higher friction. Figure 3.7 shows the section profile for rough tungsten before and after the friction tests It can be seen that the asperities on the rough tungsten surface are slowly worn down as the experiment progresses. The behavior of tungsten can be explained by the fact that the softer tungsten/tungsten oxide undergoes plastic deformation at the points of contact of the asperities, and thus wears more easily. As a result, localized removal of material takes place at the points of contact, which results in changes in its surface morphology. Solution chemistry does not seem to play critical role in the process, as no discernible effects were observed by changing solution pH or ionic strength.

Solution Chemistry Effects for SiO_2

The operating pressure and velocity for this study were the same as those in the previous section. The pH values that were tested were 3.0, 7.0 and 11.0. The ionic strength levels were 10^{-3}, 10^{-2} and 1.0 M (at pH 11.0). Fig. 3.2 shows the surface morphology of the silica samples used for the experiments. The effect of solution pH for the silica samples is shown in Figure 3.8. Lowest frictional forces were observed for pH 11.00. When solutions of pH 7.00 and 3.00 were used, higher frictional forces were observed, with the largest increase occurring at the transition from pH 11.00 to 7.00. This indicated that as the pH was reduced, the asperities on the wafer surface started interacting more strongly with the pad surface, resulting in a higher measured frictional force. This is believed to be due to the decrease in electrostatic repulsion between the wafer and pad surface at lower pH. Most metal oxides have a surface layer of metal hydroxide, which can become positively or negatively charged depending on the pH, based on the following mechanism:

$$M-(OH) + H^+ \Leftrightarrow M-(OH_2)^+ \quad \text{(positive at low pH)} \quad (3.3)$$

$$M-(OH) + OH^- \Leftrightarrow M-(O)^- + H_2O \quad \text{negative at high pH)} \quad (3.4)$$

The above equations show that as pH increases, the metal oxide surface acquires a stronger negative charge. However, in practice, it is very hard to measure the actual charge on the surface. This is because in solution, oppositely charged counterions adsorb on the oxide surface and reduce the potential in its vicinity. Beyond this strongly adsorbed layer of ions, the counterion concentration tails off till it approaches the bulk concentration. This region is called the diffuse double layer. Additionally, there is a layer of solvent around the surface which can be assumed to be fixed to it. Some distance away from the surface, the liquid begins to move with respect to the solid. The potential that is most often measured (on particles as well as flat surfaces) is that of the shear plane in this diffuse double layer, where the liquid first begins to move with respect to the solid surface. The reason for this is that this shear plane potential is what another surface "sees" when it approaches another charged surface. This potential is called the electrokinetic potential or the Zeta potential [Hun93]. For SiO_2, the isoelectric pH is around 2-3. As a result, it can be said with reasonable certainty that the wafer surface is negatively charged at pH 7 and 11, and has a slightly negative or zero charge at pH 3. To determine the charge on the pad surface, streaming potential measurements were carried out on IC 1000 pad pieces . The results indicated the presence of a negative charge on the pad surface, and as the pH was increased from 4.00 to 9.00, the Zeta Potential increased from -8 mV to -25 mV, indicating a behavior similar to that of silica. From this data, it can be said that when solution pH was increased, both the wafer and pad surfaces developed a strongly negative charge and experienced significant electrostatic repulsion. As a result, the interaction between their asperities was reduced, resulting in a decrease in frictional force between the two surfaces.

The effect of ionic strength of solution (at pH 11.00) is shown in Figure 3.9. As the solution ionic strength was increased from 10^{-3}M to 1.0M, frictional forces also increased significantly. This is due to the fact that as ionic strength increased, the additional counterions introduced into the solution compress the electrical double layer around the pad and wafer surface. As a result, the Zeta potential of both surfaces decreases, and this causes a reduction in the electrostatic repulsion between them [Hun93], resulting in stronger contact between their asperities, and thus a higher frictional force.

Effect of Pressure and Velocity

This section presents some results on the effect of pressure, velocity and pad condition on the friction between the pad and wafer.

The first study shows the effect of pressure and velocity on the friction force for SiO_2. The pressure was varied from 14.4 to 43.5 kPa, and the velocity was fixed at 2.19 m/s. The friction force as a function of pressure is shown in Figure 3.10. It clearly shows that as the applied pressure increases, the real area of contact between the interacting surfaces (pad and wafer) increases, This leads to greater interaction between the asperities on their surfaces, resulting in an increase in friction force.

The second study on the effect of platen velocity was conducted at a pressure of 29.0 kPa, and the velocity was varied from 1.46 m/s to 4.39 m/s. The results are shown in Figure 3.11, and illustrate the transitions between different lubrication modes. McGrew [McG74] has reviewed the four types of slider bearing operation. These are dry operation, boundary lubrication, mixed-film lubrication and full-film lubrication. Boundary lubrication involves the presence of thin lubricating films coating the sliding surfaces; however, there is some amount of solid contact such that both solid and liquid lubricant properties are involved in the friction and wear behavior of the system. If lubrication is effective in preventing solid to solid contact, then fluid-film lubrication is said to be in effect. Mixed-film lubrication is a combination of full-film and boundary lubrication. These three regimes are often represented as a function of sliding velocity by the Stribeck Curve, which is shown in Figure 3.12. It can be seen that Fig. 3.11 shows very similar behavior, and indicates that the earlier measurements were carried out in the boundary lubrication regime, where both solid and liquid properties affect the frictional interactions between the wafer and pad surface. Additionally, these measurements also show that the friction force technique can be used to get a fairly accurate picture of the mode of fluid flow and solid-solid contact under different conditions of polishing. Also, the same experiment, when conducted on a degraded pad, i.e. one which had been worn down by extensive polishing experiments and had been subjected to additional (deliberate) wearing and was no longer polishing effectively, showed an entirely different behavior. In the velocity range of the instrument, the pad seemed to be in the full-film lubrication regime throughout. This is somewhat in agreement with earlier results reported by McGrew [McG74], which are shown in Figure 3.12. They show that surface roughness plays an important role in determining the position of the different zones on the Stribeck curve. Smoother surfaces, which have smaller asperities, tend to move from the boundary lubrication regime to the mixed-film and full-film regimes at lower velocities. The broken-in surface has had its asperities removed or smoothed over, and shows a transition to fluid film lubrication at lower velocities. Since the degraded pad shows lower friction, it can be assumed to have a smoother (glazed) surface, which has been shown by earlier researchers [Jai94], [Ste97]. In the case of the degraded pad, the region of boundary and mixed-film lubrication probably lies in a lower velocity regime, which cannot be accessed by the present instrument. However, the present results show the potential of this technique to measure pad degradation and lifetime.

Summary

This chapter has presented some results on in-situ friction force measurements, utilizing a novel in-situ apparatus developed at the University of Florida. The technique has been shown to be sensitive to sample surface roughness, and to changes in roughness during the experiments. Additionally, the effect of solution chemistry parameters like pH and ionic strength on friction forces in the silica system was also demonstrated. The change in friction under different chemistries was shown to be due to changes in the electrostatic interactions between the pad and wafer surface under different conditions of pH and ionic strength. Finally, the influence of the condition of the polishing pad was also shown. This was demonstrated by conducting friction experiments for different pad velocities, and the transition form boundary lubrication to fluid film lubrication was shown to be dependent on the condition of the pad. These results indicate that this technique holds promise as an in-situ monitor for the CMP process.

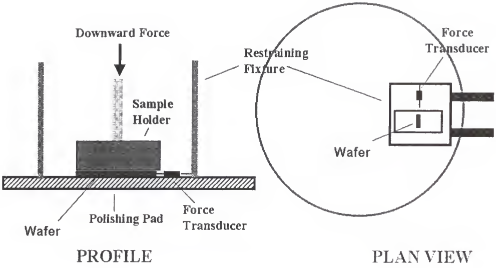

Figure 3.1: Schematic outline of Friction Force Measurement Apparatus

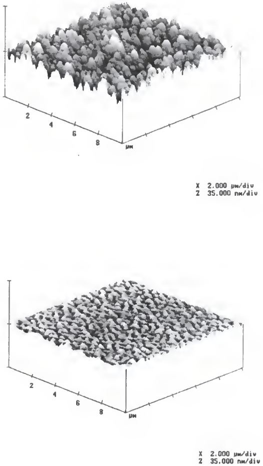

RMS: 2.65 nm
R_{max}: 23.22 nm

RMS: 0.88 nm
R_{max}: 7.94 nm

Figure 3.2: AFM Micrographs of Silica films of two different roughnesses

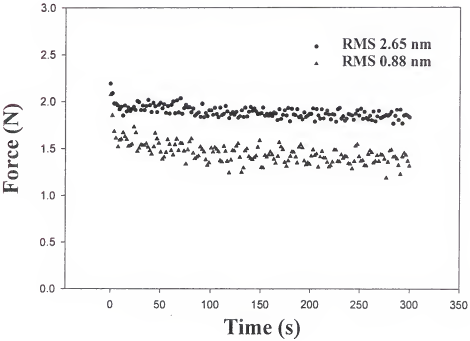

Figure 3.3: Friction force response for silica surfaces of two different roughnesses

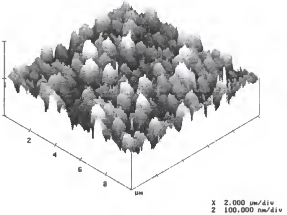

RMS: 13.75 nm
R_{max}: 121.4 nm

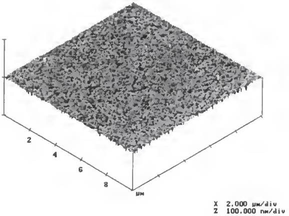

RMS: 1.83 nm
R_{max}: 22.69 nm

Figure 3.4: AFM Micrographs of unpolished and polished Tungsten surfaces before the friction measurements

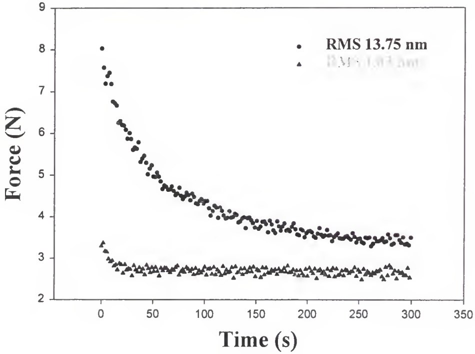

Figure 3.5: Friction force response for rough (unpolished) and smooth (polished) Tungsten films

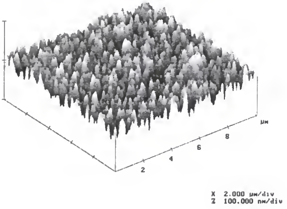

RMS: 11.92 nm
R_{max}: 83.00 nm

Figure 3.6: AFM Micrograph of rough Tungsten surface after the friction experiments

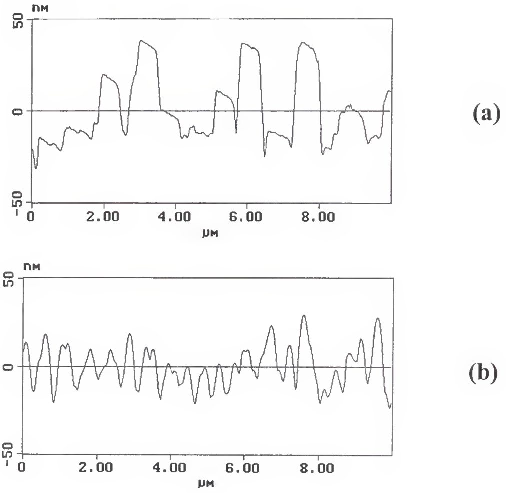

Figure 3.7: Section analysis of Tungsten film (a) before and (b) after the friction experiments

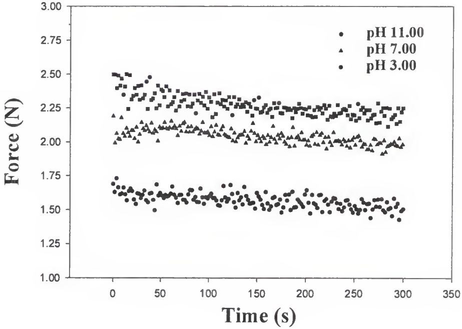

Figure 3.8: Effect of solution pH on friction forces for Silica

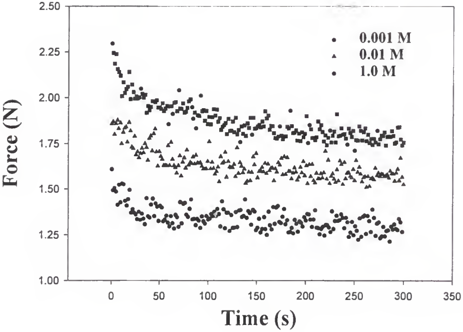

Figure 3.9: Effect of solution Ionic Strength on friction forces for Silica

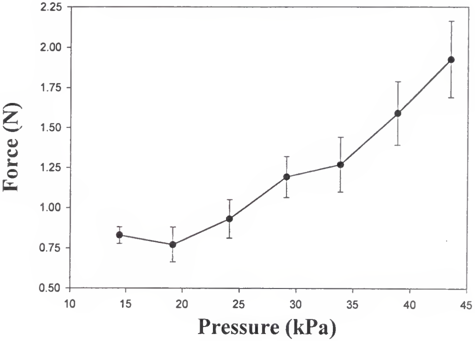

Figure 3.10: Friction force for Silica as a function of applied pressure

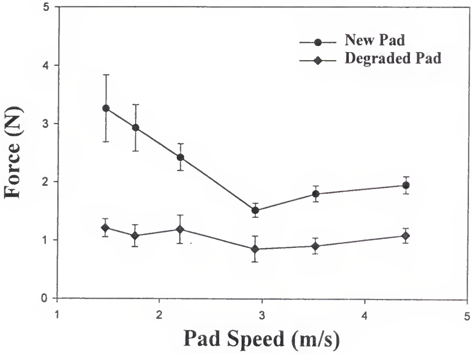

Figure 3.11: Friction force as a function of pad velocity for new and degraded pads

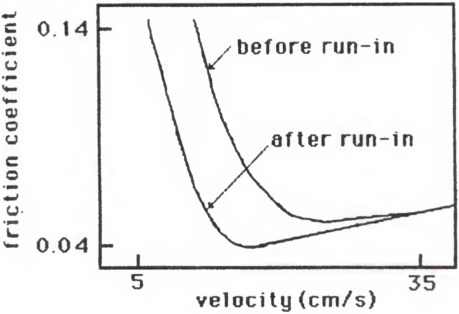

Figure 3.12: Stribeck curve, showing variation of friction coefficient with velocity for surfaces with two different roughnesses [McG74]

CHAPTER 4
EFFECT OF PARTICLE SIZE

Introduction

As has been explained in Chapter 2, the effect of abrasive size in polishing has been studied by several researchers, who have obtained different and often contradictory trends. This is partly due to the fact that very few systematic studies have been conducted on the effect of both particle size and concentration. One such study was conducted by Bielmann [Bie98] on Tungsten CMP. The results of that study clearly showed that polishing rate in tungsten shows an inverse dependence on particle size. This chapter presents the results of a similar study on SiO_2 CMP.

Materials and Methods

The samples used for the CMP experiments were obtained from 8 inch diameter p-type <100> silicon wafers, on which 2.0 µm thick SiO_2 films had been deposited by Plasma Enhanced Chemical Vapor Deposition (PECVD), using Tetraethoxysilane (TEOS) as the precursor. 1.0 inch x 1.0 inch squares were then cut from these wafers and used as samples for the polishing experiments. Sol-gel silica particles of four different sizes

(0.2, 0.5, 1.0 and 1.5 µm diameter) were obtained from Geltech Corporation. These particles are highly spherical and have a narrow size distribution, making them ideal for such a study. The size and shape of these particles was characterized by electron microscopy and particle size analysis. Scanning Electron Microscopy using a JEOL JSM 6400 SEM was used to characterize the three larger sizes, while Transmission Electron Microscopy using a JEOL 200 CX TEM was used to characterize the 0.2 µm particles.

Ellipsometry

The thickness of the SiO_2 films was measured by using Variable Angle Spectroscopic Ellipsometry (VASE). A J.A. Woollam Spectroscopic ellipsometer was used for this purpose. This technique measures the change in polarization state of light reflected from the surface of a sample. Fundamentally, ellipsometry refers just to the measurement of the polarization state of a light beam. However, these measurements are usually performed in order to describe an "optical system" that modifies the polarization state of a light beam. The measured values are expressed as psi (Ψ) and delta (Δ). These values are related to the ratio of Fresnel reflection coefficients Rp and Rs for p- and s- polarized light, respectively.

$$\rho = \frac{R_p}{R_s} = \tan(\Psi)e^{i\Delta} \tag{3.1}$$

Because ellipsometry measures the ratio of two values it can be highly accurate and very reproducible. Also, because the ratio is a complex number, it also contains "phase" information (Δ), which makes the measurement very sensitive. Ellipsometry can be used to determine film thicknesses, thin film optical constants, and in many cases both thickness and optical constants of the same film.

Ellipsometry, like all optical techniques, does not directly measure layer thicknesses or optical constants. What is does is measure polarization states, possibly as functions of the light wavelength, angle of incidence and/or polarization state. The measured data is then fit to an optical model. This model contains some known parameters, such as the wavelength of the incident light, the incident beam polarization state and the angle of incidence. The model should also contain some unknown physical constants such as layer thickness and optical constants. These unknown parameters are varied and the resulting data from the model is compared to the experimental data till a good fit is obtained. For a more detailed explanation of the technique is provided in the manual [Woo97].

Slurry Preparation

The slurries for the polishing experiments were prepared by adding a known amount of the particles to deionized (DI) water. The solids loading was varied from 0.25 to 15.0 % by weight. After adding the particles, the pH was adjusted to 10.5, which is in the range used for SiO_2 CMP. The particles were then dispersed by using ultrasonic energy and mechanical agitation. Bath sonicators were used for this purpose. The smaller particles were more aggregated, and took longer to disperse. Particle size analysis was used to confirm the quality of dispersion and to verify the particle size as observed by microscopy.

Particle Size Analysis

The size analysis was conducted using a Honeywell Microtrac UPA 150 Particle Size Analyzer. This instrument utilizes the technique of dynamic light scattering. In this instrument, a few drops of dispersed suspension (enough to give a strong scattering signal) of the particles to be analyzed is added to a cell containing water adjusted to an optimum pH for particle stability. The suspended particles undergo random collisions between themselves and the thermally excited molecules of the fluid (Brownian Motion). The velocity distribution of these particles is a known function of particle size, and of other factors such as temperature and viscosity of the fluid. For a given set of conditions, smaller particles have a larger velocity than larger particles. Higher temperature and lower viscosity also result in higher particle velocities. Light from a laser diode is passed through the sample, and the light scattered from each particle is Doppler-shifted by the Brownian motion of the particles. This scattered light is then combined with a reference (unscattered) beam from the same source in a silicon photodetector. The detector output is then amplified, filtered, digitized and mathematically analyzed by the software to recover the particle size distribution. This is known as Homodyne detection. Following the size analysis, the pH of the slurries was readjusted to 10.5 right before the polishing experiments.

Setup for Polishing

The setup for the CMP experiments is shown in Figure 4.1(a). A Struers Rotopol 31 polisher, along with a Struers Multidoser slurry feed system and a Struers Rotoforce 3 polishing head was used for conducting all the polishing experiments. The Rotopol unit has a 12 inch diameter platen on which the polishing pad is mounted. The pads used for the experiments were IC 1000/Suba IV stacked pads, obtained from Rodel Corporation. This is a standard configuration used by the CMP industry, the reasons for which have been explained in

Chapter 2. The Multidoser unit consists of several peristaltic pumps which are used to transport the slurry to the pad. The Rotoforce unit is the polishing head in which the sample holder is mounted. Pressure is applied pneumatically, and the polishing time and pressure can be set to desired values. The sample holder is schematically illustrated in Figure 4.1(b). It is a 2.25 inch diameter stainless steel cylinder, with a height of 1.13 inches. A flat square recess (1 inch x 1 inch x 0.03 inch) is machined in the center of one of the flat surfaces. The recess constrains the wafer mechanically during polishing, preventing it form sliding out or moving. A backing material (40 film, obtained from Rodel) is mounted inside the recess. It brings the wafer slightly (0.05 inch) above the flat sample holder surface, and is made wet before the sample is put on it, in order to hold the wafer using capillary forces. Additionally, it provides some backing flexibility to compensate for local variations in pad thickness during polishing. The experimental conditions were set as follows: the sample and pad rotation speeds were fixed at 150 rpm (translating to a linear velocity of 1.4 m/s), the downward force was set at 7.0 psi (48.4 kPa), and the sample was offset by 3.5 inches from the center of the pad. After polishing, the samples were ultrasonicated in DI water (pH 10). This provides mechanical energy to dislodge slurry particles from the wafer surface, and the alkaline pH enhances electrostatic repulsion between the two surfaces as well.

The polishing rate was determined by measuring the thickness of the films in the central region after polishing. The difference in thickness was used to determine the polishing rate. The surface morphology and roughness of the polished samples was characterized by Atomic Force Microscopy (AFM).

Results and Discussion

Experimental Results

Polishing rate

Figure 4.2 shows the electron Micrographs of the four types of particles used in this study. It can be seen that the particles are indeed extremely spherical, and have a fairly narrow size distribution. A representative light scattering size distribution for the four particle sizes is shown in Figure 4.3. As can be seen, the size distribution is quite narrow, and corresponds quite well to the manufacturer's specifications. Figure 4.4 shows the variation in polishing rate with solids concentration for the four particle sizes. It can be seen that there is an optimum concentration for each particle size, and this optimum shifts to lower values as particle size increases. The range of optimum concentrations also narrows significantly with increase in particle size. When compared with the earlier results obtained by Bielmann [Bie98] on Tungsten CMP, these results clearly show the difference in the nature of the two processes. CMP requires surface modification to ensure high removal rates and good surface quality. In the case of Tungsten, this is accomplished by adding an oxidizer to the slurry, which forms a very thin film (few angstroms) of Tungsten Oxide on the surface, which is then removed by the mechanical action of the abrasive particles. In this case, since a very thin film of oxide is to be removed, the extent to which the particles penetrate the surface is not as critical as the frequency of abrasion. A high frequency of abrasion is desired so that the particles remove the oxide film when it is very thin and is forming rapidly, so that high oxidation rates are maintained. In SiO_2 CMP, on the other hand, the modification of the surface is brought about not by an oxidizing chemical, but by the mechanical pressure of the particles themselves, which cause water to diffuse into the near-surface region of the substrate, making it softer and more easily removable.

Surface morphology of polished samples

The surface morphology of the polished samples was also characterized by Atomic Force Microscopy (AFM). The results for the samples polished with 2 wt.% slurries are shown in Figure 4.5. The AFM images and sections show that at low solids loading, increasing particle size causes an increase in roughness, which is to be expected. Very little to no surface damage was observed for those samples. Figure 4.6 shows the images and sections of the samples polished with the 15 wt.% slurries. The larger particle sizes (0.5, 1.0 and 1.5 μm) caused significant pitting on the silica surface. These pits were also observed for the samples polished with 5 wt.% and 10 wt.% slurries of the 1.0 and 1.5 μm particles, and for the samples polished with 10 wt.% slurries of the 0.5 μm particles. From the polishing rate curves, it can be seen that pit formation is coincident with a reduction in polish rate. Table 4.1 shows the average number of pits, pit diameters and pit depths obtained from multiple AFM images of the samples polished at 15 wt.% solids loading. The error represents the standard deviation from the average values.

Table 4.1: Average number of pits, pit diameter and pit depth for samples polished with 15.0 wt.% slurries of the four different particle sizes used in this study

Particle Size (μm)	Number of pits	Pit Diameter (μm)	Pit Depth (nm)
0.5	43 ± 7.7	0.54 ± 0.18	8.21 ± 3.92
1.0	19.5 ± 2.9	0.95 ± 0.24	16.6 ± 10.4
1.5	5.7 ± 1.15	1.94 ± 0.59	37.5 ± 18.6

It can be seen clearly that the number of pits reduces and the pit depth and pit diameter shows a corresponding increase with particle size. This shows a correlation to particle size (indent depth) and the number of particles in the slurries (number of pits). This could be due to the reduced pressure on the larger particles under high solids loading conditions causes reduced (localized) material removal and dissolution of silica, which shows up as pits on the oxide surface. In addition, because the unpolished surfaces (blanket SiO_2) are very smooth to begin with (<0.3 nm RMS roughness), the effect of the polishing particles would be to initially roughen the surface. Due to the reduced polishing rate, this roughness is then not reduced significantly by subsequent abrasion.

From the above results, it can be seen that the pressure per particle is a critical factor in determining the extent of mechanical removal and chemical surface modification it can cause. To delineate the chemical and mechanical aspects of removal, a model is presented in the next section. Although it is not complete, it can provide some trends to explain the variation in polishing rates with abrasive concentration and size.

Theoretical Model

The model is based on previous work on abrasion and contact mechanics, using the principles of Hertzian

Indentation [Joh85] and the model developed by Cook [Coo90].

The first step in the procedure is determining the number of particles participating in the polishing process. This is determined by estimating the number of abrasives per unit volume of the slurry.

$$N = \frac{C}{\rho \cdot \pi \cdot \frac{d^3}{6}} \qquad (4.1)$$

where N is the number of particles per unit volume, C is the mass concentration of particles per unit volume, ρ is the density of the particles and d is the particle diameter.

Mechanical removal

From the number of particles, the load per particle can be estimated. This is given by the total force applied on the substrate divided by the number of particles

$$f = \frac{F}{N} \qquad (4.2)$$

where F = 34 N. Additionally, Chauhan et al. [Cha93] have shown that very few (1 in 10^5) particles are actually involved in active polishing or wear. Including that factor in calculating the number of particles, and using the expressions developed by Hertz for elastic indentation of a particle into a flat substrate, the mechanical depth of penetration is given by the following expression

$$\delta_m = \left(\frac{9 \cdot f}{8 \cdot d \cdot E^2}\right)^{\frac{1}{3}} \tag{4.3}$$

where E is the Young’s modulus of the substrate and is equal to 72 GPa for SiO_2. From this, the indent volume per particle is given by

$$V_{mp} = \frac{\pi}{3} \cdot \delta_m^2 \cdot \left(\frac{3 \cdot d}{2} - \delta_m\right) \tag{4.4}$$

The total indent volume is then determined by multiplying the indent volume per particle by the total number of particles.

$$V_m = V_{mp} \cdot N \tag{4.5}$$

Plots of V_m as a function of concentration for the four different particle sizes are shown in Figure 4.7. It can be seen that the indent volume decreases with abrasive concentration and increases with abrasive size. Additionally, the indent volume for the smaller particles is around two orders of magnitude smaller than that for the largest particles. This shows that material is not being removed by purely mechanical means.

Chemical modification of surface

Since SiO_2 CMP is known to be caused by surface modification of the substrate to form a softer "gel layer", we need to determine the extent of surface modification caused by the abrasive particles. The approach of Cook [Coo90] has been used in this regard. Firstly, from Hertzian mechanics, the radius of contact between the particle and the substrate is given by

$$r_c = \left(\frac{3 \cdot d \cdot f}{8 \cdot E}\right)^{\frac{1}{3}} \tag{4.6}$$

The contact pressure per particle is then given by

$$p_c = \frac{f}{\pi \cdot r_c^2} \tag{4.7}$$

To determine the extent of water diffusion due to the stress imposed by the particles, the dwell time of the particle-wafer contact must be estimated. It is defined as

$$t_c = \frac{2 \cdot r_c}{v_p} \tag{4.8}$$

where v_p is the particle velocity (which is the relative velocity between the pad and wafer) and is equal to 1.4 m/s for the conditions used in this study.

The local coefficient of friction between the two surfaces is defined as

$$\mu = \frac{F_f}{f} \tag{4.9}$$

where f is the normal force, and F_f is the frictional force at the local particle-substrate interface and is defined as

$$F_f = \frac{\pi \cdot r_c^2 \cdot f_b \cdot E}{10} \tag{4.10}$$

where πr_c^2 is the contact area between the two surfaces, f_b is the fraction of the contact area in which bonding occurs (~0.01) and E/10 is an estimate for the theoretical fracture strength of the SiO_2 network bonds.

According to Nogami and Tomozawa [Nog84], water diffusion is exponentially enhanced under conditions of tensile stresses. So, to estimate the tensile stress at the trailing edge of the particle, the relationship developed by Lawn and Wilshaw [Law75] for a traveling Hertzian indenter was used.

$$\sigma_t = p_c \cdot \left(\frac{1 - 2\nu}{2}\right) \cdot \left(1 + c_2 \cdot \nu\right) \tag{4.11}$$

where ν is the Poisson's ratio for SiO_2 and is equal to 0.16, and c_2 is given by the following expression:

$$c_2 = \frac{[3 \cdot \pi \cdot (4 + \nu)]}{[8 \cdot (1 - 2\nu)]} = 7.207 \tag{4.12}$$

The effective diffusion coefficient for water in SiO_2 is given by the following expression:

$$D_{eff} = D_0 \cdot \left(e^{\frac{\sigma_t \cdot V_d}{R \cdot T}} + e^{-\frac{\sigma_t \cdot V_d}{R \cdot T}} \right) \tag{4.13}$$

to account for the compressive stresses at the leading edge and the tensile stresses at the trailing edge. D_o is the zero stress diffusion coefficient and is equal to 10^{-17} m^2/s, V_d is the activation volume for diffusion and is equal to $1.7x10^{-4}$ m^3, R is the gas constant, and T is the temperature at the interface during polishing (assumed to be =465 K).

The time under this tensile load is equal to the dwell time of contact t_c. Therefore, the diffusion depth for water is given by the expression

$$\delta_c = \sqrt{2 \cdot D_{eff} \cdot t_c} \tag{4.14}$$

and the total (chemical + mechanical) modified volume is given by the expression

$$V_{c+m} = \frac{\pi}{3} \cdot \left[\left(\delta_m + \delta_c \right)^2 \cdot \left(3\frac{d}{2} - \delta_m - \delta_c \right) \right] \cdot N \qquad (4.15)$$

Therefore the chemically modified volume is given by

$$V_c = V_{c+m} - V_m \qquad (4.16)$$

Figure 4.8 shows the plots of diffusion depth for the four particle sizes as a function of particle concentration. Figure 4.9 shows the chemically modified volume as a function of concentration. It can be seen that the modified volume is very large for the larger particles at low solids concentrations, and tends to drop sharply at higher concentrations. On the other hand, for the smaller particles, the modified volume tends to increase with particle concentration for the smaller sized abrasives. Since this modified volume controls removal to a large extent, this could be one of the reasons for fall-off in polish rate for large particles at higher concentrations, and for the increase in removal rate of the smaller particles. Another factor that must be borne in mind is that the effect of the polishing pad has not been considered in this treatment. It is a fact that at low particle, concentrations, most of the load is borne by the pad and not by the particles. As more particles are added to the system, a greater proportion of the load is carried by them, and this is what is responsible for the initial increase in polishing rates at low concentrations, even for the larger particles.

Contact area

Another factor that influences polishing rate is the total area of contact of the abrasives and the substrate, as that determines the degree of dissolution of SiO_2 and the extent to which the dissolved and abraded material will adsorb to the particles and be carried away from the substrate. Figure 4.10 shows the contact area between the two surfaces, and Figure 4.11 shows the total surface area of the particles as a function of concentration. It can be clearly seen that the smaller particles have a much greater contact area, and the total surface area is also larger by a very large degree for the 0.2 μm particles. This could be responsible for ensuring high removal rates at high solids concentrations for the smaller particles. This is especially important because redeposition of material has been observed quite often in SiO_2 and glass polishing [Coo90].

All these results imply that at low concentrations, the larger particles have a high degree of surface modification. This results in higher polishing rates under low solids loading conditions, because of the larger volume of easily removable material. At higher concentrations, the extent of chemical modification reduces to the point that only localized dissolution of SiO_2 takes place around the vicinity of the particles. This results in formation of etch pits on the wafer surface. The smaller particles, on the other hand, are more effective at modifying the surface under higher solids concentrations, and their higher surface area also aids in more effective dissolution and transportation of dissolved products away from the substrate. This makes up for their lower mechanical abrasion, and results in higher polishing rates at high concentrations.

This model is not yet complete, and does not include several parameters like the interaction of the particles with the pad surface, and how particle size influences the load distribution between the pad and particles. This, along with rheological studies on these suspensions under CMP-like conditions, can help refine this model and make it more accurate.

Summary

A systematic study on the effect of particle size and concentration on SiO_2 CMP was conducted. The results show that larger particles are more effective at polishing under low concentrations, and their effectiveness drops at higher concentrations. Smaller particles show the opposite behavior. Calculations show that this is possibly due to the enhanced effectiveness of the smaller particles at modifying the SiO_2 surface at high concentrations, and also due to their larger contact area, which promotes enhanced dissolution and provides a larger surface for the dissolution and abrasion products to adsorb on and be carried away from the wafer surface during polishing. With larger particles, on the other hand, at high concentrations, their effectiveness at modifying the surface is reduced, and their surface area is not high enough to promote high rates of material transport away from the wafer surface. As a result, only localized dissolution and etching occurs around the particle-wafer interface, showing up as pits on the polished surface.

Finally, from a process standpoint, the experimental results show that to obtain a robust polishing process which gives good surface quality and is relatively insensitive to fluctuations in particle concentration, it is better to use large concentrations of smaller abrasives as opposed to small amounts of larger abrasives, as the resulting process gives both high removal rates and good surface finish.

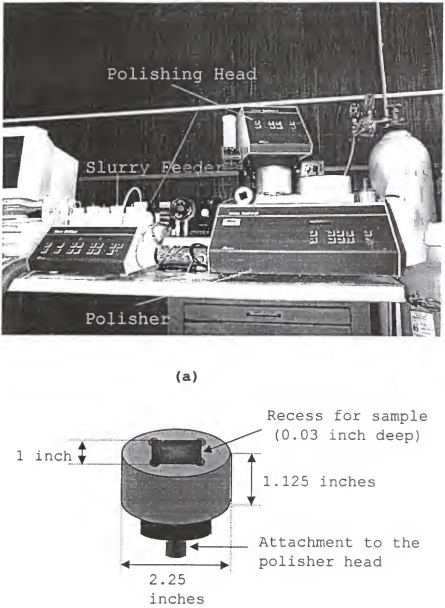

Figure 4.1: (a) Setup for the polishing experiments (b) Schematic of sample holder used for polishing

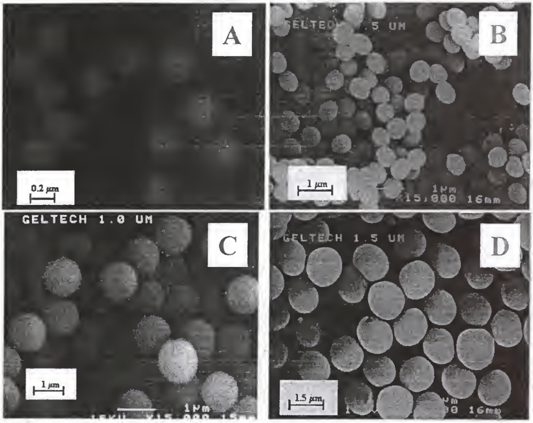

Figure 4.2: Electron Micrographs of (A) 0.2 µm (B) 0.5 µm (C) 1.0 µm and (D) 1.5 µm diameter SiO_2 particles

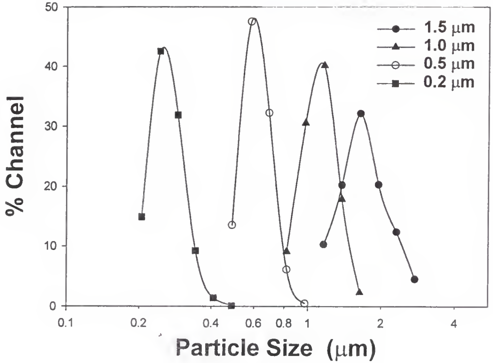

Figure 4.3: Size distributions for SiO_2 particles obtained by Dynamic Light Scattering

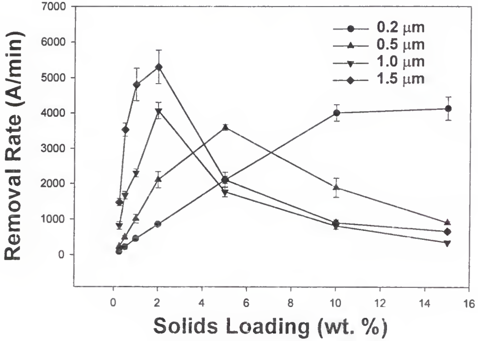

Figure 4.4: SiO_2 polishing rates as a function of solids loading for 0.2, 0.5, 1.0 and 1.5 μm diameter SiO_2 particles

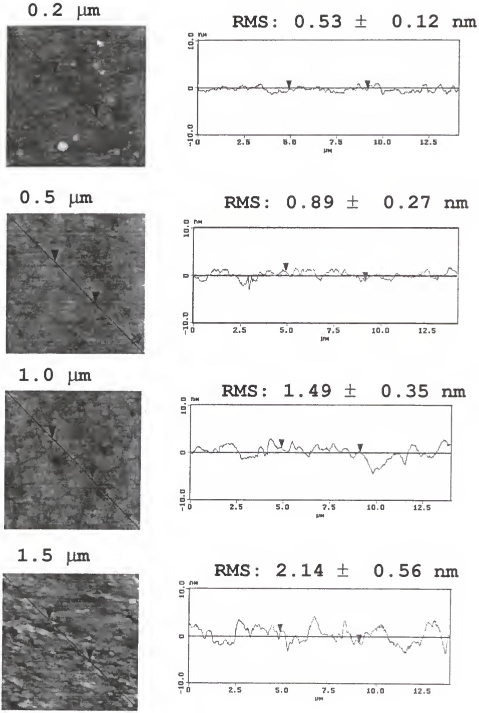

Figure 4.5: AFM micrographs and sections of samples polished with 2.0 wt.% slurries of SiO_2 particles

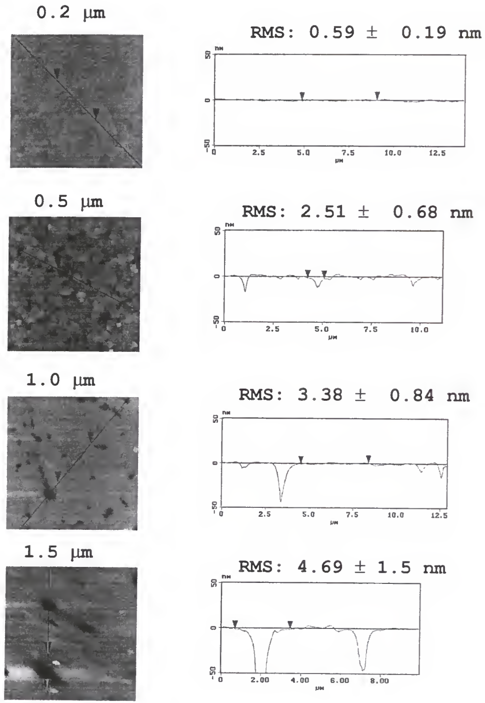

Figure 4.6: AFM micrographs and sections of samples polished with 15.0 wt.% slurries of SiO_2 particles

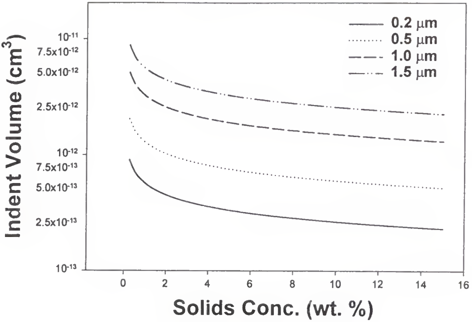

Figure 4.7: Calculated Total Indent Volume as a function of concentration for different particle sizes

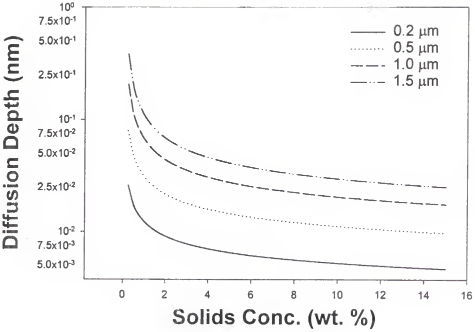

Figure 4.8: Calculated Diffusion depth of water as a function of concentration for different particle sizes

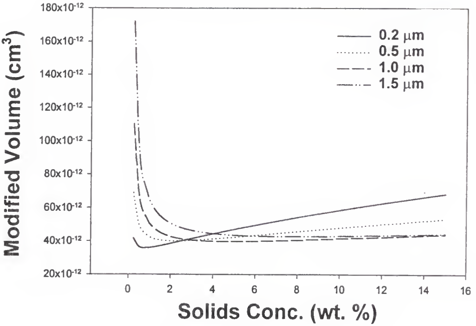

Figure 4.9: Calculated total modified volume as a function of concentration for different particle sizes

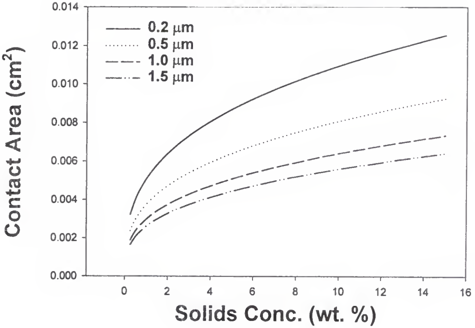

Figure 4.10: Calculated Contact area between particles and wafer as a function of concentration for different particle sizes

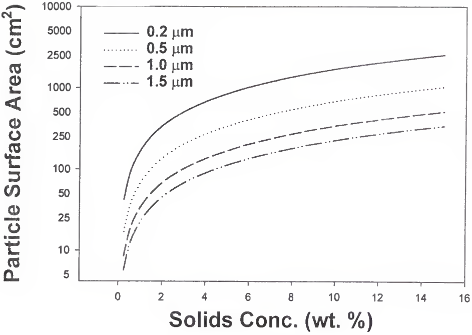

Figure 4.11: Calculated surface area of particles as a function of concentration for different particle sizes

CHAPTER 5
EFFECT OF SLURRY IONIC STRENGTH

Introduction

In the absence of adsorbed surfactants or polymers, the stability of a dilute oxide suspension is maintained by electrostatic repulsion due to particle surface charge. The particle-particle repulsion can be reduced by ionic screening or counterions which are held in an interfacial layer surrounding the particle. If this screening is sufficient, particle having sufficient kinetic energy will be able to more easily surmount this repulsive barrier and physically bond as a result of Van der Waals attractive forces. Thus, at a given pH, one can destabilize most dilute oxide suspensions by increasing the ionic strength with an inert electrolyte [Hie86]. All CMP polishing slurries contain additives of different types. Some are added to enhance dissolution or etch rates, some as oxidizers, some as chelating agents and so forth. These additives often increase the ionic strength of the slurry, which can have undesirable consequences for slurry stability. This can affect slurry lifetime, and also decrease process yield by introducing defects on the polished surface. These defects are usually caused by large particles, which are generated as a result of agglomeration of the primary particles in the slurry. As a result, most slurries also contain dispersing agents to keep them stable over long periods of time.

This study focuses on the effect of adding different amounts of alkali metal salts (LiCl, NaCl and KCl) on polishing rate and surface quality of SiO_2 films. The salt addition is then correlated to slurry stability via particle size, Zeta Potential and turbidity (settling) tests. From these results, and from earlier results on friction force experiments, an explanation is then presented.

Materials and Methods

ACS grade LiCl, NaCl and KCl were used in this study. The salts were obtained from Fisher Scientific. 0.2 µm Geltech SiO_2 particles were used as the abrasives in all the experiments. The abrasive concentration was fixed at 5.0 % by weight, and the slurries were dispersed in the manner described in Chapter 4. Following the dispersion, the slurry pH was adjusted to 10.50. The salt was then added, dissolved, and the pH was readjusted to 10.50. The polishing conditions were the same as described in the previous chapter.

The new characterization techniques used in this study are as follows:

Particle Size Analysis

A Coulter LS 230 light scattering instrument was used for analyzing particle size as a function of salt concentration in the slurry. Light with a wavelength of 750 nm is used for this purpose. The measurement is accomplished by measuring the pattern of light scattered by the constituent particles in the sample. The scattered light as a function of scattering angle is used to form a diffraction pattern. Each particle's diffraction pattern is characteristic of its size. The individual patterns from the many moving particles are superimposed using a Fourier lens to create a single composite diffraction pattern, which is measured by detectors. Over the measurement, a running average is computed of the flux patterns at every instant. The analysis of this pattern then yields the particles distribution of the sample. This technique can give size information for particles from 0.4 µm to 2000 µm in size. For smaller particles, another technique called PIDS (Polarization Intensity Differential Scattering) is used. It is based on a property of light called polarization. For particles in the size ranges close to the wavelength of light, the difference in scattering of vertically versus horizontally polarized light, when the scattering is observed at roughly right angles to the direction of propagation of light, depends sensitively on the

---

ratio of particle size to the wavelength of the light wave. The PIDS assembly uses three sets of horizontally and vertically polarized filters to provide polarized monochromatic light at three different wavelengths, viz. 450 nm, 600 nm and 900 nm. The PIDS assembly measures the pattern of the difference in scattering of vertically and horizontally polarized light. The particle are sequentially illuminated with light of the three different wavelengths. For each of the three wavelengths, the differential scattering pattern is measured by six detectors. The difference in scattering between the two polarizations for all three wavelengths is then added to the same matrix that is used for diffraction sizing, and the relative volume of particles for each size channel is determined by solution to this matrix. The reason for using this instrument for this study, as opposed to the Microtrac UPA 150, is that the suspensions being analyzed are not always stable, and would probably settle in the stagnant sample cell of the UPA 150. In the LS 230, however, a stirring arrangement is present, which enables us to keep the particle suspended, and to simulate the shear conditions of the polishing process to some degree.

Zeta Potential

For determining the Zeta Potential of the SiO_2 particles as a function of salt concentration, a Colloidal Dynamics

Acoustosizer was used. This instrument applies an alternating electric field at megahertz frequencies (0.3-11.0 MHz) to the dispersion, which generates a sound wave. This is called the Electrokinetic Sonic Amplitude (ESA) effect. The effect arises because the particles in the suspension move backwards and forwards due to the applied signal. However, there is a phase lag between the signal and the resulting response because of the inertia of the particles. The ions in the surrounding double layer, however, are able to keep up with the signal even at high frequencies. The measured ESA signal is directly related to a quantity called the dynamic mobility of the particles. From this quantity, it is possible to calculate the particle size and effective electric charge on the particle surface. The phase lag as a function of the frequency of the applied field can be used to determine the particle size. Also, since the phase lag is often independent of the charge on the particles, the size can be used to determine the charge or Zeta potential of the particles [OBr95]. The instrument is schematically illustrated in Figure 5.1. The electric field is applied in the form of a short pulse, lasting only a few microseconds, across the two electrodes. The sound wave which is generated in the suspension travels down the glass rod and is detected by the transducer at the end.

The chief advantage of this instrument is that it can be used to analyze concentrated dispersions, thus removing the need for sample dilution. Additionally, titrations can be performed to determine the isoelectric point of the particles. The main limitations of this technique are that it can provide size information only for particles between 0.1 and 10.0 µm in size. Additionally, it assumes that the particles have a log-normal size distribution.

Turbidity Measurements

Turbidity of a suspension can be used as an index of its stability. Suspensions that transmit less light show higher turbidity values. If a suspension is unstable, it will tend to settle over time, and this will result in a decrease in its turbidity. As a result, monitoring the variation of this parameter can give a simple index of the suspension stability. A Hach Model 2100AN Laboratory Turbidimeter was used for this purpose. It measures turbidity from 0 to 10,000 Nephelometric Turbidity Units (NTU). Its optical system consists of a tungsten filament lamp, lenses and apertures to focus the light, a forward-scatter light detector, a transmitted-light detector and a back-scatter light detector. It also utilizes a "Ratio" mode, which uses a mathematical calculation to ratio signals from each detector. This gives it a wide range of measurements, calibration stability, excellent linearity and the ability to measure turbidity in the presence of color. In this measurement, the sample is placed in a clean and dry cell, which is then further cleaned on the outside by silicone oil to remove fingerprints, dust and other sources of error. The cell is then placed in the unit, and the measurements are carried out automatically for the time desired.

Results and Discussion

Polishing Rate and Surface Morphology

Figure 5.2 shows polish rate as a function of salt concentration for the three different salts. It can clearly be seen that addition of salt causes a significant enhancement of polish rates. This is expected to be due to formation of large aggregates in the slurry, which are formed as a result of the reduced repulsion between the abrasive particles in the presence of salt, causing them to come together. The deeper penetration and gouging caused by these larger particles should result in increased roughness of the polished surface. However, from Figure 5.3, it can be seen that this is not the case. Even under conditions of 1.0 M salt, the roughness of the polished surface is comparable to that of the surface polished by slurry containing no salt. Similar results have been reported by us earlier for tungsten CMP [Bie99a] [Bie99b], where we have shown that polishing with slurries containing 0.1 M oxidizer (potassium ferricyanide) results in very smooth surfaces, although $K_3Fe(CN)_6$ is a multivalent salt and coagulates the alumina slurry in very small amounts. This implies that the shear stresses imposed by the polishing process are sufficient to break any aggregates formed by adding salt, and that these larger particles are not responsible for the higher wear rates.

Zeta Potential, Turbidity and Particle Size

Zeta potential results shown in Figure 5.4 show that addition of salt suppresses the electric double layer around the silica particles and reduces their surface charge, making them more likely to agglomerate . The figure only shows the results of measurements carried out till salt concentrations of 0.5 M, as further additions of the salt increased the background electrolyte concentration to the point where the measurement error was beyond acceptable limits. However, at 0.5 M salt it can be seen that the reduction in zeta potential is greater for LiCl and NaCl as compared to KCl. This suggests that these two salts are more effective at coagulating the slurry than KCl. These results were confirmed by turbidity measurements, which showed no significant decrease in turbidity over a period of two hours after adding 0.01 M and 0.1 M salt. However, addition of 1.0 M salt resulted in rapid coagulation of the slurries, as can be seen from Figure 5.5, with the coagulation effectiveness of the three salts being as follows: LiCl >NaCl > KCl. In addition, particle size measurements as a function of salt concentration showed that no coagulation occurred till a salt concentration of 0.5 M, when NaCl started to coagulate the slurry particles. At 1.0 M salt, all three salts caused coagulation of the slurry. However, LiCl was the most effective coagulant at this concentration, followed by NaCl and KCl. This can be seen in Figure 5.6, which shows a representative particle size distribution for each salt at 1.0 M. LiCl and NaCl shift the particle size distribution to a larger extent than KCl.

Several researchers have conducted studies on the relative effectiveness of alkali metal ions in coagulating silica dispersions. Tien [Tie65] studied the adsorption of alkali metal cations on silica gel, and obtained the affinity sequence $Cs^+ > Rb^+ > K^+ > Na^+ > Li^+$. He stated that this was due to the fact that the smaller ions, being more hydrated, are not able to enter the fine pore structure of the gel surface, and consequently adsorb less efficiently. Tadros and Lyklema [Tad67] obtained the same sequence ($Li^+ < Na^+ < K^+ < Cs^+$). They interpreted their results in a similar manner as Tien. Allen and Matijevic [All70] obtained the same sequence for colloidal silica at low pHs, and their interpretation for this behavior was that ion exchange of the counterions in exchange for the release of protons occurs at the silica surface. The smaller the solvated (hydrated) volume, the more pronounced is the tendency to ion exchange. However, for pHs higher than 10, the sequence started to change, and higher amounts of K^+ and Cs^+ were required to coagulate the suspensions. Their explanation for this phenomenon was not very clear. Depasse and Watillon [Dep70] observed that all the alkali metal cations could coagulate the silica dispersions between pHs of 7-11, but only Li^+ and Na^+ were able to bring coagulation above pH 11. They postulated that between pH 7 and 11, the particles tend to form bonds with each other through interactions between basic (dissociated) $Si-O^-$ species and acidic Si-OH species. This made it relatively easy to induce coagulation. For pH >11, the silica surface is essentially covered with basic groups, and only strongly hydrated (acidic) ions like Li^+ and Na^+ can induce coagulation. Recently, Colic et al. [Col98] used settling and viscosity measurements to show that LiCl and NaCl are more effective than KCl in coagulating silica slurries at high salt concentrations and high pH. These are conditions similar to those utilized in this study. The interpretation of the authors is that the smaller and more strongly hydrated Li ions have a greater affinity towards the surface hydration region on the silica surface, and thus penetrate it more deeply to neutralize the charge on the particle surface.

As can be seen from the above discussion, the exact reason for the variation in coagulation effectiveness of these different ions is not yet clear, and a more detailed discussion is beyond the scope of this thesis. What can be said from the results of this study is that the increased removal rate due to salt addition is not due to any agglomerates that may be present in the slurry, as the lower salt concentrations do not cause any observable coagulation, and yet lead to significant enhancement in removal rate. That, along with the low roughness of all the polished samples, suggests that the enhanced wear rate is primarily due to increased contact between the surfaces participating in the polishing process. It is well known that silica surfaces (wafer and particles) have a strong negative charge at alkaline pH, and it has been determined as a part of another study (Chapter 3) that the pad surface is also negatively charged under these conditions [Mah99b]. Due to addition of salt to the system, the alkali metal counterions compress the electrical double layer around the particles, wafer and pad surfaces, which reduces the electrostatic repulsion between them, thus increasing the effective contact between the particles, wafer and pad. This enhanced contact thus results in higher removal rates. Similar results have been obtained in the measurement of frictional forces between a SiO_2 wafer and polishing pad, where it has been shown that higher ionic strength solutions lead to higher friction and consequently higher removal of material from the wafer surface. This interpretation is also supported by the Zeta potential, particle size and turbidity results, which show that at higher salt concentrations, KCl is less effective at reducing Zeta potential as well as at coagulating the slurries. This explains the relatively smaller increase in removal rate in the slurries containing 1.0 M KCl, as compared to LiCl and NaCl.

Summary

The results of this study indicate that in the short term, addition of electrolytes to a polishing slurry may cause agglomeration, but the agglomerates are not detrimental to the quality of the polished surface. Additionally, the enhanced polishing rate due to salt addition has been shown to be primarily due to enhanced mechanical interactions between the surfaces participating in the polishing process. This has been interpreted as being due to the reduced electrostatic repulsion between the negatively charged particles, pad and wafer surface under high salt conditions. The effectiveness of a salt in coagulating the suspensions showed a direct correlation to the enhancement in polish rate, especially at high salt concentrations.

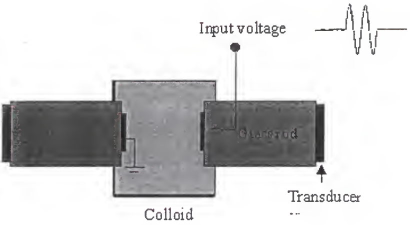

Figure 5.1: Schematic illustration of Acoustosizer [OBr95]

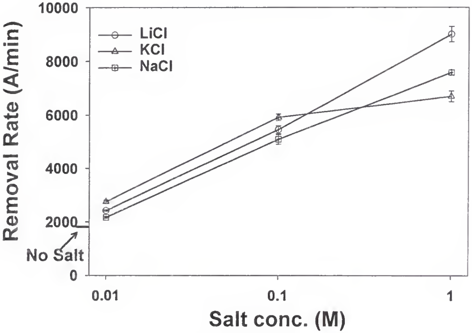

Figure 5.2: SiO_2 Polishing Rate as a function of salt concentration for LiCl, NaCl and KCl

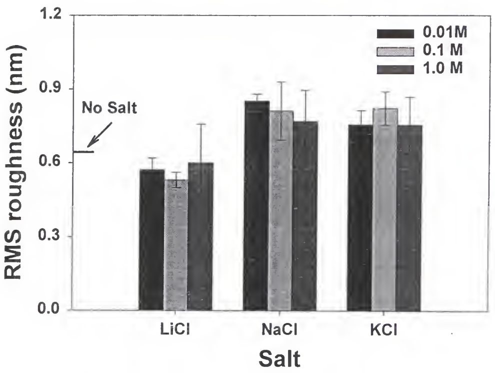

Figure 5.3: RMS roughness of polished samples for different salt concentrations

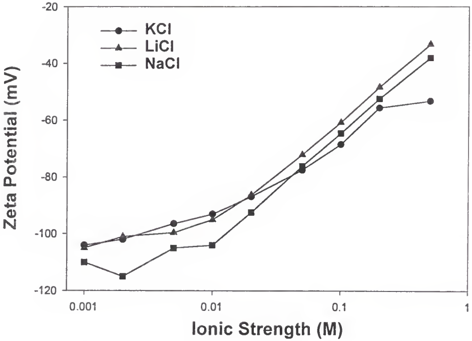

Figure 5.4: Zeta Potential as a function of Ionic Strength for SiO_2 suspensions containing LiCl, NaCl and KCl

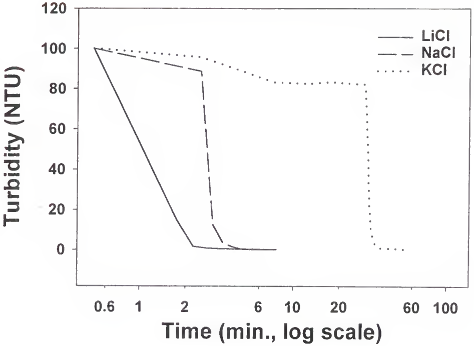

Figure 5.5: Normalized turbidity of SiO_2 suspensions containing 1.0 M salt as a function of time

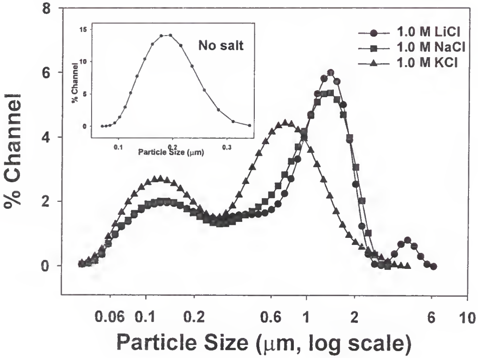

Figure 5.6: Particle size distribution of SiO_2 suspensions containing 1.0 M Salt (Inset: Particle size distribution of stable suspension)

CHAPTER 6
EFFECT OF ABRASIVE MATERIAL PROPERTIES

Introduction

The nature of the abrasive itself plays a critical role in its efficiency of removing material, as well as the resulting quality of the polished surface. Properties such as the hardness and density of the abrasive and the material of which it is composed are still not well characterized in terms of their effect in polishing. Cook [Coo90] has summarized the present knowledge base in this area, and has also indicated that understanding of these parameters is still inadequate. Ramarajan et al. [Ram99] have done some experiments on polishing different materials with alumina particles of different densities, but their experimental parameters were incorrectly defined. Other than that, some researchers [Jai94] have presented results on the use of Cerium Oxide (CeO_2) for oxide CMP, and recent work on STI CMP using CeO_2 slurries has shown promising results, as CeO_2 shows a high selectivity towards Silicon Nitride as compared to SiO_2 slurries. The reason for this is still not very clear, though.

This study involves the use of abrasives of different materials properties (density, different abrasive materials) for SiO_2 CMP. The abrasives chosen have a similar size distribution, and approximately similar morphology. Polishing experiments were conducted as a function of slurry pH for the selected abrasives, to delineate the effect of the isoelectric point (IEP) and density of the abrasives on their polishing characteristics. Although many of the results are preliminary, interesting trends have been obtained, which can be the basis for future work in this area.

Materials and Methods

Abrasives of different types were selected for this study. Firstly, alumina abrasives of different densities were obtained from Ferro Corporation. These powders were prepared from the precursor Boehmite (AlOOH)by firing it to different temperatures to obtain different levels of porosity and to control the phase of the material. Following the firing, the material was then ground in a wet ball mill to its final size. These powders were characterized in detail in terms of particle size, density and surface area. The last two parameters give fairly good index of the hardness of these materials, as it is impossible to do hardness testing of such fine sub-micron sized particles. The particle size of these powders was estimated by using Dynamic Light Scattering, and their density and porosity was also characterized. The density of the abrasives was determined by Gas Pycnometry, and their surface area was characterized by Nitrogen BET adsorption. Prior to conducting the density and surface area measurements, the powder samples were dried overnight in a vacuum oven to remove any adsorbed moisture and organics.

Particle Density

An Ultrapycnometer-1000, manufactured by Quantachrome Corporation, was used to measure the density of the powders used in this study. The instrument uses Archimedes' principle of fluid displacement and Boyle's law to determine the volume. The displaced fluid is a gas which can penetrate the finest pores, thereby assuring maximum accuracy. Helium gas is used for this purpose, since its small atomic dimensions assures penetration into crevices and pores approaching 1 Å in dimension. Its behavior as an ideal gas is also desirable. The measurement is accomplished by placing the sample (powder) in the sample cell and adding He gas to it till a certain overpressure. Following this, a solenoid valve is opened and an additional volume is added to the system, causing the gas pressure to drop to a lower value. From the measured pressures, and knowing the cell volume (which is periodically calibrated using stainless steel standard spheres), the volume of sample can be calculated. From this and the measured sample mass, the density is then determined. A more detailed explanation of the procedure and the derivation of the formulas used to determine the volume is provided in the manual.

Surface Area

The surface area of these powders was determined by Nitrogen adsorption, using a Quantachrome Nova 1200 Gas Sorption Analyzer. In this technique, the sample holder is partly immersed in a coolant (liquid Nitrogen) and evacuated. Nitrogen gas is then transferred into it, and based on the amount of gas required to achieve a specific cell pressure, the number of moles of nitrogen can be estimated. The sample cell is calibrated in its empty condition too, so that the amount of gas adsorbed on the powder can be determined. For these measurements, the Brunauer-Emmett-Teller (BET) method was used, which uses the following equation:

$$\frac{1}{W \cdot [\frac{P_0}{P} - 1]} = \frac{1}{W_m \cdot C} + \frac{C - 1}{W_m \cdot C} \cdot (\frac{P}{P_0} \qquad (6.1)$$

In which W is the weight of gas adsorbed at a relative pressure P/P_0 and W_m is the weight of adsorbate constituting a monolayer of surface coverage. The term C is the BET constant, which is related to the energy of adsorption in the first adsorbed layer. Consequently its value is an indication of the magnitude of adsorbent/adsorbate interactions. From a linear plot of $1/[W(P_0/P)-1]$ vs. P/P_0, W_m is determined, from which the surface area of the sample is calculated by using the cross-sectional area of the adsorbate (Nitrogen) molecule. The specific surface area of the solid is then calculated by dividing the total surface area by the sample mass.

Additionally, Zirconia (ZrO_2), from Ferro Corporation, Titania (TiO_2) and Alumina particles obtained from Nanophase Corporation, and Silica (SiO_2) from Geltech Corporation were also characterized. For these abrasive particles, size and Zeta potential measurements were carried out. Particle size analysis was carried out using the Microtrac UPA 150, and Zeta potential measurements were carried out using the Acoustosizer. Both these instruments have been described in earlier chapters.

The polishing slurries were prepared using the method described in Chapter 4. The solids concentration was maintained at 2.0% by volume. Polishing experiments were conducted at pH 4 and 11 for the alumina particles of varying density. For the other particles, polishing experiments were conducted at four pHs, viz. 3, 6, 9 and 11. The conditions used in polishing were the same as those described in previous chapters. However, for the second part of this study, where different materials were compared for their polishing characteristics, a different sample holder was fabricated. This was because when polishing experiments were conducted at pHs close to the abrasive IEP, the wafer samples were not stable inside the holder, and this resulted in significant damage to their surface from chipping and scratching. Due to this, a new sample holder was fabricated, in which the samples were glued to Aluminum squares, which were then held against the backing film of a different sample holding chuck. This prevented sample movement during the experiment, and eliminated the problem of wafer chipping.

The polishing rate was determined by ellipsometry, and AFM was used to characterize the morphology of the polished samples. For the second part of this study, X-ray Photoelectron Spectroscopy (XPS) was used for surface chemical analysis of the polished samples, and Scanning Electron Microscopy (SEM) was used to characterize the particle deposition on the wafer surface.

Results and Discussion

Effect of Abrasive Density

Table 6.1 shows the properties of the Al_2O_3 particles used in this study, and Table 6.2 shows the properties of the different phases of alumina present in these particles. The compositional analysis of the materials was obtained from the manufacturer (Ferro Corporation).

Table 6.1: Properties of alumina particles of different densities

Sample ID	Crystal Phase	Median Particle Size (μm)	Density (g/cm^3)	B.E.T. Surface Area (m^2/g)
A	> 90% γ	0.25	2.99	118.12
B	> 90% δ/θ	0.18	3.22	79.34
C	85-90% α	0.21	3.57	46.49
D	90-95% α	0.19	3.86	26.18

Table 6.2: Properties of the different phases present in the alumina particles [Git70]

Phase	Crystal System	Angle	Unit Cell Parameters		
γ	Tetragonal		7.95	7.95	7.79
δ	Tetragonal		7.97	7.97	23.47
θ	Monoclinic	103°42	5.63	2.95	11.86
α	Hexagonal		4.76		12.99

It can clearly be seen that the density of these powders shows an increase which corresponds to the phase sequence in the thermal transformation characteristics of Al_2O_3 (Figure 6.1). The γ-Al_2O_3 powder has the lowest density, followed by the powder containing 90% δ/θ phase. The samples containing predominantly α-Al_2O_3 are the densest. Additionally, the denser samples also have the smallest surface area. Figure 6.2 shows the variation in surface area with density of the powders. Since the particle size of these samples is similar, it can be safely assumed that the difference in surface area is due to the relative amounts of porosity in these materials. Additionally, it is well known that the hardness of Al_2O_3 increases as its phase changes from γ to α [Git70], although the absolute values of the measured hardness vary significantly. Figure 6.3 shows TEM micrographs of the particles. The size and shape of the particles corresponds fairly closely to that measured by the Light Scattering instrument.

The results of the CMP experiments conducted at pH 4 and 11 are shown in Figure 6.4. It can be seen that the polish rate shows an increase with particle density. This increase is also more pronounced at pH 11. The pH effect can be explained by the fact that the solubility of SiO_2 increases by several orders of magnitude beyond pH 9. This makes the surface softer and more easily removable, and also enhances the solubility of the reaction and abrasion products coming out of solution, as has been explained in earlier sections. The increase in polishing rate with abrasive density shows that a denser powder of the same material is more effective at polishing. This is not only due to its ability to better penetrate and remove material, but also due to its higher mechanical integrity. The reason for this statement is that while conducting AFM analysis of the samples after polishing, the samples polished with abrasives A and B had very high levels of particulate contamination, and required additional cleaning. The reason for this could be that these materials, being less densified, are more friable and tend to fragment and deform on the surface of the samples during polishing, thus leading to larger numbers of particles on the wafer surface.

AFM micrographs of the samples polished with these abrasives are shown in Figures 6.5 and 6.6. Samples polished with abrasive D show significant damage and pitting on their surfaces. Some slight damage is also observed on the samples polished with abrasive C. However, the samples polished with abrasive D at pH 11 show much more damage. This is again due to the enhanced dissolution of SiO_2 at this pH, and confirms the important role played by stress-enhanced dissolution in obtaining high polishing rates. The solubility of Al_2O_3 is also known to increase at pHs below 4 and beyond pH 9. However, this is expected to be similar for the different samples, and should not cause any significant relative changes to their abrasive properties.

These results clearly illustrate how particle properties such as density, phase and porosity can be tailored to obtain control of their abrasive behavior. This can be especially useful in the area of CMP of Copper and low-k dielectrics, which are soft materials and tend to get easily scratched and damaged. By utilizing a suitable abrasive, not only can controlled removal rates be obtained, but the surface finish of the polished material can also be significantly improved.

Effect of Abrasive Material

Table 6.3 shows the properties of the different materials used in this study.

Table 6.3: Properties of different powders used in this study

Powder	Crystal Phase	Median Particle Size (μm)	Density (g/cm^3)	IEP (pH)
Silica	Amorphous	0.2	2.2	3.0
Alumina	Tetragonal	0.12	3.6	9.4
Titania	Tetragonal	0.15	3.95	6.0
Zirconia	Monoclinic	0.15	5.58	9.0

The results showing the polishing rate for Nanotek Al_2O_3 particles as a function of slurry pH are shown in Figure 6.7(a). The polishing rate was highest at pH 11, and almost no polishing took place at lower pHs. Additionally, the samples polished at pH 9 had a hazy deposit on their surface, which could not be removed even by strong mechanical cleaning (scrubbing). Surface chemical analysis using XPS showed a strong Al^{3+} peak for these samples, as can be seen from Figure 6.8. The other samples had some residual Al_2O_3 as well, but the concentration was much lower. This behavior is unexpected, especially because the level of contamination at the IEP is higher than that observed at pH 3 and 6, when the two surfaces (Al_2O_3 and SiO_2) are oppositely charged. Comparing the polishing data to the surface charge on the Al_2O_3 particles (Figure 6.7(b)), we see that the polishing rate drops to zero at the IEP of the abrasives (pH 9.2). Similar behavior was seen for TiO_2 and ZrO_2 abrasives as well. Figure 6.9 shows that the polish rate for TiO_2 drops to zero at pH 6, which is its IEP, and the same phenomenon can be seen for ZrO_2 at pH 9 (Figure 6.10). Significant particulate contamination was observed for these two abrasives as well, although it was not as severe as it was for the samples polished with Alumina particles.

The reason for this phenomenon are not clear, and understanding it completely will require significant additional research. However, one possible reason could be the so-called "chemomechanical effects" in materials, which have been studied for several years. Westwood [Wes73a], [Wes80] has summarized much of the work in this area. Several researchers have shown correlations between the Zeta potential of a material and its hardness. The variation of pendulum hardness of Al_2O_3 with Zeta potential was studied by Westwood et al. [Wes73b]. They showed that Al_2O_3 was hardest and most effectively drilled at its IEP. Additional studies on hardness correlations of various materials to their Zeta potential have been described in the reviews by Westwood. The reasons for this phenomenon are still not fully understood. Various hypotheses include a minimum in the dislocation mobility at the IEP. Support for this argument is provided by results obtained by MacMillan et al. [Mac73], who conducted etch-pitting studies on the movement of edge and screw dislocations around hardness indentations in freshly cleaved MgO surfaces. The reason for this could be that the mobility of dislocations in ionic crystals is controlled predominantly by interactions with point defects like impurity atoms and vacancies. The surface charge resulting from chemisorption can cause bending or tilting of energy bands at the surface, and in certain circumstances, this can alter the distribution of electrons in the energy levels associated with the dislocation cores. Such adsorption-induced changes in the electronic state of near-surface point defects can then cause variations in their mutual interactions, which then manifest as environmentally induced changes in dislocation mobility, and hence, hardness [Wes80].

This variation in hardness with Zeta potential could thus be responsible for enhanced particle hardness. Because of this, the particles penetrate the surface of the SiO_2 film and get embedded in it, forming a layer which then prevents any polishing from taking place. SEM micrographs of the wafer surfaces after polishing under these conditions seem to bear out this interpretation. Figure 6.11 shows very large Al_2O_3 particle deposition, and the TiO_2 particles also show significant deposition, although on a reduced scale.

The same experiments, when conducted with SiO_2 abrasives, showed significantly different results, though. Figure 6.12 shows the variation in polish rate with SiO_2 slurry pH. It can clearly be seen that the polishing behavior follows a trend similar to that for the solubility of Silica. Polishing rate is highest under alkaline conditions, as expected. However, as the pH approaches the IEP of the abrasives (pH 3) the polishing rate started increasing again, which is probably due to the increasing solubility of silica under these conditions. The reason for this "anomalous" behavior is not understood yet. However, it must be borne in mind that SiO_2 is a fairly unique material as compared to most other metal oxides. It is amorphous, and it is the only metal oxide which is reasonably stable at its IEP [Ile79]. This stability has been hypothesized to be due to hydration forces, which provide short-range repulsion in the absence of electrostatic repulsion, thus keeping the particles apart [Col98]. Due to the following reasons, its properties cannot be expected to be representative of crystalline compounds like Al_2O_3, TiO_2 and

ZrO_2, and more work is required before a definitive mechanism for the above observations is formulated.

Summary

This study showed how polishing rates can be tailored by controlling abrasive properties like phase, density and porosity. Denser abrasives containing a harder phase of alumina polished SiO_2 more aggressively than less dense particles. Additionally, the denser abrasives also caused more significant damage to the sample surface.

Polishing with different abrasive materials illustrated how material properties change with slurry pH. The severe particle adhesion observed at the IEP is attributed to change in abrasive hardness, which causes the particles to penetrate into the SiC_2 surface and form a layer which prevents further polishing. However, this behavior was not observed for SiO_2 abrasives, showing that more work is required to fully understand this phenomenon.

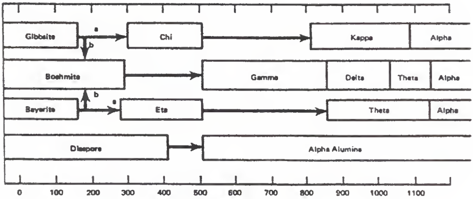

Figure 6.1: Thermal transformation characteristics of Alumina [Git70]

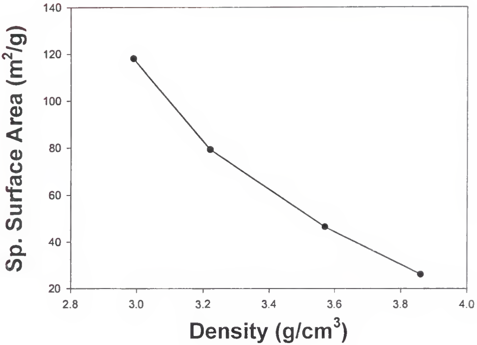

Figure 6.2: Specific surface area of Alumina particles as a function of particle density

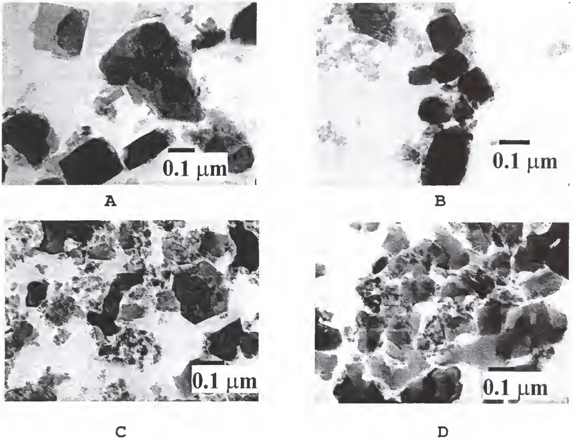

Figure 6.3: TEM Micrographs of Alumina particles from samples A, B, C and D

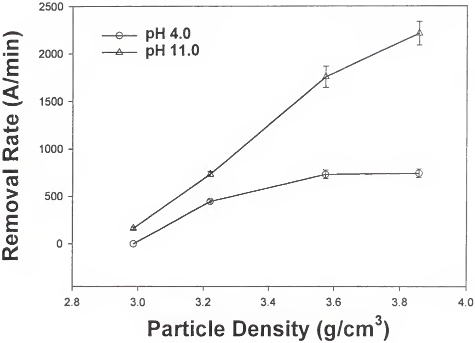

Figure 6.4: SiO_2 polishing rate as a function of Alumina particle density for pH 4 and 11

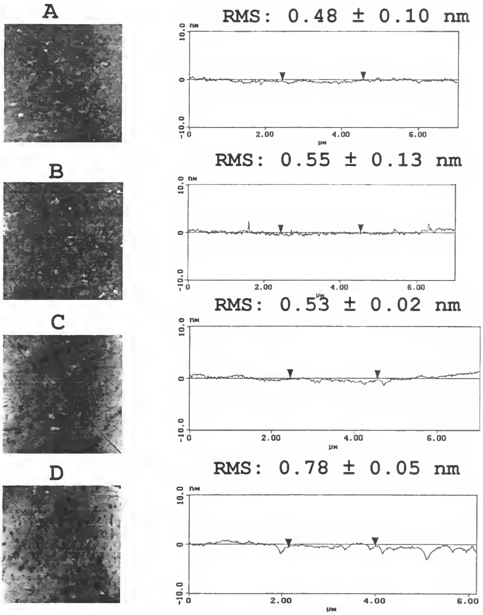

Figure 6.5: AFM Micrographs of samples polished with Alumina slurries at pH 4

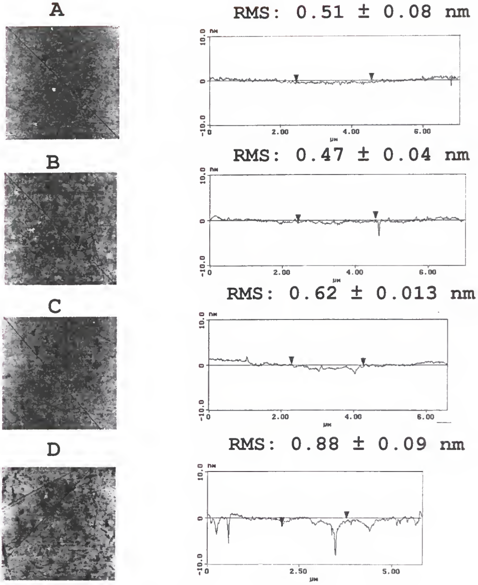

Figure 6.6: AFM Micrographs of samples polished with Alumina slurries at pH 11

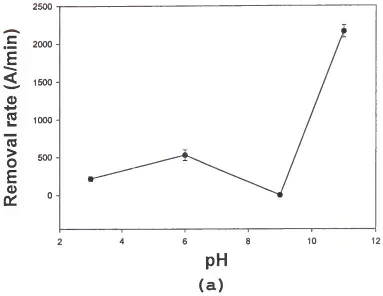

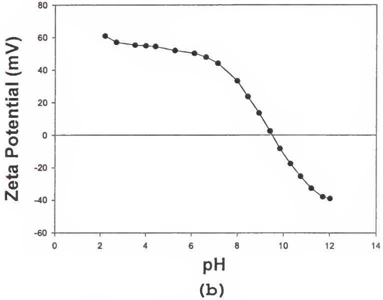

Figure 6.7: (a) SiO_2 polishing rate as a function of Al_2O_3 slurry pH (b) Zeta Potential of Al_2O_3 particles as a function of pH

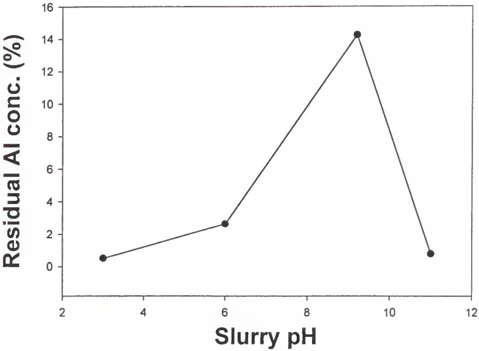

Figure 6.8: XPS surface analysis of residual Alumina on wafer surface after polishing at different pHs

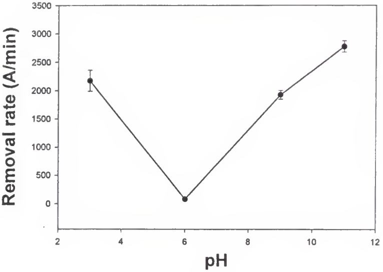

(a)

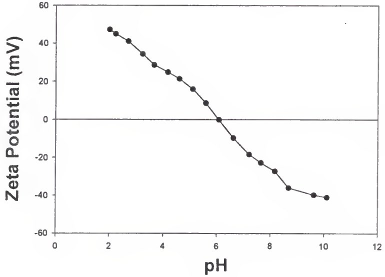

(b)

Figure 6.9: (a) SiO_2 polishing rate as a function of TiO_2 slurry pH (b) Zeta Potential of TiO_2 particles as a function of pH

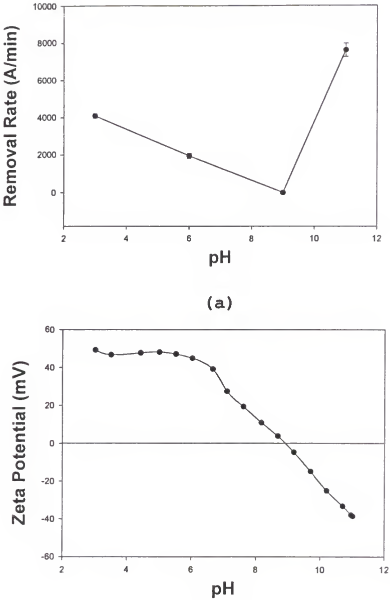

(a)

(b)

Figure 6.10: (a) SiO_2 polishing rate as a function of ZrO_2 slurry pH (b) Zeta Potential of ZrO_2 particles as a function of pH

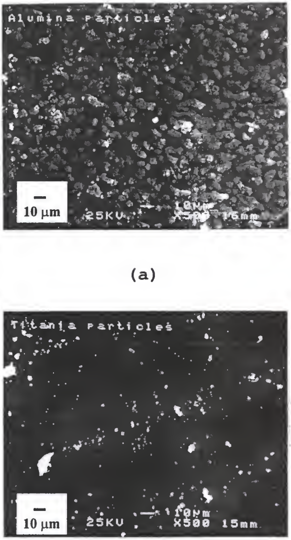

(a)

(b)

Figure 6.11: SEM micrographs of wafer surfaces after polishing with (a) Alumina and (b) Titania particles at their respective IEPs

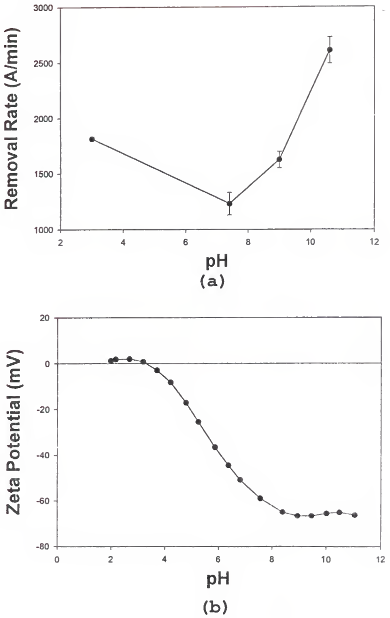

Figure 6.12: (a) SiO_2 polishing rate as a function of SiO_2 slurry pH (b) Zeta Potential of SiO_2 particles as a function of pH

CHAPTER 7
CONCLUSIONS

In this study, Chemical Mechanical Polishing (CMP) experiments were conducted with a view to characterizing the effect of abrasive properties on SiO_2 CMP. Additionally, a novel in-situ friction force apparatus was also used to study wafer-pad interactions.

The friction force measurements showed the effect of surface roughness on interactions between the wafer and pad. Additionally, it was shown that by changing the chemistry (pH, ionic strength) of the solutions used in these measurements, the electrostatic force between the two surfaces can be modified, which shows up as a change in their frictional interactions. Additionally, by monitoring the friction force as a function of polishing pad velocity, it was shown that the condition of the pad determines the transition from boundary layer lubrication to full fluid-film lubrication. A degraded pad showed fluid film lubrication over the entire velocity range of the instrument. All these measurements show that the technique holds promise as a tool for process monitoring and for understanding wafer-slurry-pad interactions during polishing as well. Future work which is in progress includes developing a new setup which rotates during the experiments, so that actual polishing can be conducted along with the friction measurements, and developing the technique further for process monitoring, especially pad degradation measurements.

Studies on the effect of particle size and density showed that an optimum concentration exists for each particle size. This optimum shifts to lower concentrations and becomes narrower as particle size increases. The reason for this has been attributed to a reduced ability of the larger particles to both mechanically remove material, and to a degradation in their ability to chemically modify the substrate by promoting the diffusion of water into its near surface region. The smaller particles, on the other hand, show a slight increase in their chemical modification ability with increase in concentration. Additionally, the smaller particles also have a much larger surface area than the larger (micron-sized) abrasives. This provides more surface for the dissolution and abrasion products to adsorb to, thus promoting the removal of material from the vicinity of the substrate and enabling higher removal rates at high concentrations. Future work in this area could include refining this model and including parameters like the interaction of the polishing pad with the particles and wafer, and including the effects of parameters like slurry viscosity and flow behavior during the polishing process.

Studies on the effect of ionic strength of the slurries on removal and slurry stability showed that alkali metal ions (Li, Na and K) coagulate SiO_2 suspensions only at very high concentrations (around 1.0 M). However, polishing results showed enhanced polishing even on adding relatively small amounts of salt. The surface quality of the polished films was also not significantly altered by the presence of salt, showing that any large aggregates formed by coagulation are not responsible for enhanced polishing. This increase in removal rates has been attributed to enhanced mechanical interactions between the surfaces in the presence of salt, due to the screening of their negative charges by the metal cations. This results in lowered electrostatic repulsion, which causes high removal rates. Friction force measurements conducted as a function of ionic strength also support this interpretation.

Finally, the effect of alumina particle density on SiO_2 CMP was shown. The denser particles polished SiO_2 much more effectively, and also caused more damage to the surface in terms of microscratching. The particles with lower density (higher porosity) not only polished less, but also has higher levels of particle contamination. This has been attributed to their inferior mechanical properties, which probably causes them to break and deform during polishing, causing them to smear on to the SiO_2 surface. Some preliminary results on polishing with different abrasives at different slurry pHs indicate that the mechanical properties of the abrasive materials change significantly at their Iso-electric Points (IEPs), which leads to almost zero polishing, and severe particle contamination, which cannot be removed even by strong cleaning steps. There is significant potential for work in this area, especially to characterize the effects of abrasive material properties on the polishing process. This will require better polishing tools, and a more detailed characterization of the abrasive particles as well.

Finally, from all the experimental and theoretical results obtained in the course of this work, we can conclude that by modulating the physical (roughness, density, particle size) and chemical (pH, ionic strength) parameters controlling the interactions between the surfaces involved in polishing, a well-controlled polishing process can be obtained.

LIST OF REFERENCES

Ach96 K. Achuthan, J. Curry, M. Lacy, D. Campbell and S.V. Babu, J. Electron. Mater. **25** (10), 1628 (1996)

All70 L.H. Allen and E. Matijevic, J. Colloid Interface Sci. **31**, 287 (1970)

Bie98 M. Bielmann, *Chemical Mechanical Polishing of Tungsten*, Masters Thesis, University of Florida (1998)

Bie99a M. Bielmann, U. Mahajan, R.K. Singh, D.O. Shah and B.J. Palla, Electrochem. Solid-State Lett. **2**, 148 (1999)

Bie99b M. Bielmann, U. Mahajan and R.K. Singh, Electrochem. Solid-State Lett. **2**, 401 (1999)

Bor99 C.L. Borst, D.G. Thakurta, W.N. Gill and R.J. Gutmann, J. Electrochem. Soc. **146**, 4309 (1999)

Bow64 F.P. Bowden and D. Tabor, *The Friction and Lubrication of Solids*, Pt II., Oxford University Press, (1964)

Bro81 N.J. Brown, P.C. Baker and R.T. Maney, Proc. SPIE **306**, 42 (1981)

Bun94 B.C. Bunker, J. Non-Cryst. Solids **179**, 300 (1994)

Car95 R. Carpio, J. Farkas and R. Jairath, Thin Solid Films **266**, 238 (1995)

Cha93 R. Chauhan, Y. Ahn, S. Chandrashekhar and T.N. Farris, Wear **162-164**, 246 (1993)

Che99 W-C. Chen, S-C. Lin, B-T. Dai and M-S. Tsai, J. Electrochem. Soc. **146**, 3004 (1999)

Col98 M. Colic, M.L. Fisher and G.V. Franks, Langmuir **14**, 6107 (1998)

Coo90 L.M. Cook, J. Non-Cryst. Solids **120**, 152 (1990)

Coo92 L.M. Cook, in *Proc. SRC Topical Research Conf. On Chem-Mechanical Polishing for Planarization*, SRC, Research Triangle Park, NC (1992), Proc. Vol.# P92008

Cop00 J. Coppeta, C. Rogers, L. Racz, A. Philipossian and F.B. Kaufman, J. Electrochem. Soc. **147**, 1903 (2000)

Dep70 J. Depasse and A. Watillon, J. Colloid Interface Sci. **33**, 430 (1970)

Dun91 H. Dunken, J. Non-Cryst. Solids **129**, 64 (1991)

Fan00 S.J. Fang, S. Garza, H. Guo, T.H. Smith, G.B. Shinn, J.E. Campbell and M.L. Hartsell, J. Electrochem. Soc. **147**, 682 (2000)

Far95 J. Farkas, R. Carpio, R. Bajaj, C. Galanaki, R. Jairath, B.P. Jones and S.M. Tzeng, in *Advanced Metallization for ULSI Applications in 1994*, edited by R. Blumenthal and G. Janssen, Materials Research Society, Pittsburgh (1995)

Fox80 P.G. Fox, Phys. Chem. Glasses **21**, 161 (1980)

Git70 W.H. Gitzen, *Alumina as a Ceramic Material*, The American Ceramic Society, Westerville, OH (1970)

Gol91 D. Golini and S.D. Jacobs, Appl. Opt. **30**, 2761 (1991)

Gro99 M. E. Gross, R. Drese, C. Lingk, W. L. Brown, K. Evans-Lutterodt, D. Barr, D. Golovin, T. Ritzdorf, J. Turner and L. Graham, in *Polycrystalline Metal and Magnetic Thin Films*, edited by David E. Laughlin, Mat. Res. Soc. Symp. Proc. **562**, 215 (1999)

Hal75 J. Halling, *Principles of Tribology*, Macmillan Press Ltd., London (1975)

Har99 T. Hara, T. Tomisawa, T. Kurosu and T.K. Doy, J. Electrochem. Soc. **146**, 2333 (1999)

Har00 M. Hariharaputhiran, Y. Li, S. Ramarajan and S.V. Babu, Electrochem. Solid-State Lett.**3** (2), 95 (2000)

Hay92 I.P. Hayward, I.L. Singer and L.E. Seitzman, Wear **157**, 215 (1992)

Hie86 P.C. Hiemenz, *Principles of Colloid and Surface Chemistry*, Dekker, New York (1986)

Hir87 K. Hirao and M. Tomozawa, J. Am. Ceram. Soc., **70** (7), 499 (1987)

Hol64 L. Holland, *The Properties of Glass Surfaces*, Chapman & Hall, London (1964)

Hom97 Y. Homma, T. Furusawa, H. Morishima and H. Sato, Solid-State Electron. **41**, 1005 (1997)

Hun93 R.J. Hunter, *Introduction to Modern Colloid Science*, Oxford University Press, Oxford (1993)

Ile79 R.K. Iler, *The Chemistry of Silica*, John Wiley & Sons, New York (1979)

Ili80 I. Iliuc, *Tribology of Thin Layers*, Elsevier Scientific Publishing, (1980)

Izu79 T. Izumitani, in *Treatise on Materials Science and Technology*, eds. M. Tomozawa and R. Doremus, Academic Press, New York (1979)

Jac98 R. L. Jackson, E. Broadbent, T. Cacouris, A. Harrus, M. Biberger, E. Patton and T. Walsh, Solid State Technol. **41(3)**, 49 (1998)

Jai94 R. Jairath, M. Desai, R. Tolles and D. Scherber-Brewer, in *Advanced Metallization for Devices and Circuits-Science, Technology and Manufacturability*, edited by S.P. Murarka, A. Katz, K.N. Tu and K. Maex, Mat. Res. Soc. Symp. Proc. **337**, 121 (1994)

Jen94 S.P. Jeng, R.H. Havemann and M.C. Chang, *in Advanced Metallization for Devices and Circuits-Science, Technology and Manufacturability*, edited by S.P. Murarka, A. Katz, K.N. Tu and K. Maex, Mat. Res. Soc. Symp. Proc. **337**, 25 (1994)

Joh85 K.L. Johnson, *Contact Mechanics*, Cambridge University Press (1985)

Kal62 A. Kaller, Mschr. Feinmech. Opt. **79**, 135 (1962)

Kal98 C.G. Kallingal, D.J. Duquette and S.P. Murarka, J.

Electrochem. Soc. **145**, 2074 (1998)

Kau91 F.B. Kaufman, D.B. Thompson, R.E. Broadie, M.A. Jaso, W.L. Guthrie, D.J. Pearsons and M.B. Small, J. Electrochem. Soc. **138**, 3460 (1991)

Kit95 K. Kituta, Mater. Res. Soc. Bull. **20**, 53 (1995)

Kne97 E.A. Kneer, C. Raghunath, J.S. Jeon and S. Raghavan, J. Electrochem. Soc. **144**, 3041 (1997)

Kud79 N. Kudryavtseva, T. Yakovleva and G. Khodakov, Sov. J. Opt. Technol. **46**, 223 (1979)

Kuo00 H.S. Kuo and W.T. Tsai, J. Electrochem. Soc. **147**, 149 (2000)

Lan92 H. Landis, P. Burke, W. Cote, W. Hill, C. Hoffman, C. Kaanta, C. Koburger, W. Lange and S. Luce, Thin Solid Films **220**, 1 (1992)

Law75 B. Lawn and R. Wilshaw, J. Mater. Sci. **10**, 1049 (1975)

Lin99 C-F. Lin, W-T. Tseng, M-S. Feng and Y-L. Wang, Thin Solid Films **347**, 248 (1999)

Liu95 C-W. Liu, B-T. Dai and C-F. Yeh, J. Electrochem. Soc. **142**, 3098 (1995)

Luo97 Q. Luo, D.R. Campbell and S.V. Babu, Thin Solid Films **311**, 177 (1997)

Mac73 N.H. MacMillan, R.D. Huntington and A.R.C. Westwood, Phil. Mag. **28**, 923 (1973)

Mah99a U. Mahajan, M. Bielmann and R.K. Singh, Electrochem. Solid-State Lett. **2** (1), 46 (1999)

Mah99b U. Mahajan, M. Bielmann and R.K. Singh, Electrochem. Solid-State Lett. **2** (2),80 (1999)

McG74 J. McGrew, ASTM Standardization News **2**, 22 (1974)

Mes97 F. Mess, J. Levert and S. Danyluk, Wear **211**, 311 (1997)

Mur93 S.P. Murarka, *Metallization: theory and practice for VLSI and ULSI*, Butterworth-Heinemann (1993)

Mur96 S.P. Murarka, Solid State Technol. **39**, 83 (1996)

Nei96 J.M. Neirynck, G-R. Yang, S.P. Murarka and R.J. Gutmann, Thin Solid Films **447**, 290 (1996)

Nog84 M. Nogami and M. Tomozawa, J. Am. Ceram. Soc. **67** (2), 151 (1984)

OBr95 R.W. O'Brien, D.W. Cannon and W.N. Rowlands, J. Colloid Interface Sci. **173**, 406 (1995)

Ols93 J. Olsen and F. Moghadam, Planarization Techniques, in *Multilevel Metallization for Integrated Circuits*, eds. S.R. Wilson, C.J. Tracy and J.L. Freeman, Noyes Publications, Park Ridge, NJ (1993)

Pou74 M. Pourbaix, *Atlas of Electrochemical Equilibria in Aqueous Solution*, NACE, Houston, TX, 10 (1974)

Pre27 F. Preston, J. Soc. Glass Technol. **11**, 214 (1927)

Raj96 Krishna Rajan, J. Electron. Mater., **25** (10), 1581 (1996)

Ram99 S. Ramarajan, M. Hariharaputhiran, Y-S. Her and S.V. Babu, Surface Engineering **15**, 324 (1999)

Rau00 K. Rau, *Surface Modification of Biomaterials by Pulsed Laser Ablation Deposition and Plasma/Gamma Polymerization,* Ph.D. Dissertation, University of Florida (2000)

Run94 S.R. Runnels and L.M. Eyman, J. Electrochem. Soc. **141**, 1698 (1994)

Sil82 W. Silvernail, Paper WB1-1, Tech. Digest, Topical Meeting on Optical Fabrication and Technology, Optical Society of America (1982)

Sin82 A.K. Sinha, J.A. Cooper and H.J. Levinstein, IEEE Electron Devices Lett. **EDL-3**, 90 (1982)

Sin00 P. Singer, Semiconductor Intl. **22**, 56 (2000)

Siv92 S. Sivaram, M. H.M. Bath, E. Lee, R. Leggett, and R. Tolles,Proc. SRC Topical Research Conference on Chem-

Mechanical Polishing for Planarization, SRC, Research Triangle Park, NC (1992), proc. Vol. #P92008

Sjo96 S. Sjoberg, J. Non-Cryst. Solids **196**, 51 (1996)

Ste95 J.M. Steigerwald, S.P. Murarka, J. Ho, R.J. Gutmann and D.J. Duquette, J. Vac. Sci. Technol. B **13**(6), 2215 (1995)

Ste97 J.M. Steigerwald, S.P. Murarka, and R.J. Gutmann, *Chemical Mechanical Planarization of Microelectronic Materials*, John Wiley & Sons Inc. (1997)

Ste98 D.J. Stein, D. Hetherington, T. Guilinger and J.L. Cecchi, J. Electrochem. Soc. **145**, 3190 (1998)

Ste99a D.J. Stein,D.L. Hetherington and J.L. Cecchi, J. Electrochem. Soc., **146**, 1934 (1999)

Ste99b D.J. Stein, D.L. Hetherington and J.L. Cecchi, J. Electrochem. Soc. **146**, 376 (1999)

Ste99c D.J. Stein, J.L. Cecchi and D.L. Hetherington, J. Mater. Res. **14**, 3695 (1999)

Sti97 G. Stix, Scientific American **276**, 45 (1997)

Sze81 S.M. Sze, *Physics of Semiconductor Devices*, John Wiley & Sons Inc., New York (1981)

Tab79 D. Tabor, in J.E. Field (ed.), *Properties of Diamond*, Academic Press, Oxford, 1979, Chapter 10

Tad68 Th. F. Tadros and J. Lyklema, J. Electroanal. Chem. **17**, 267 (1968)

Tic99 J. Tichy, J.A. Levert, L. Shan and S. Danyluk, J. Electrochem. Soc. **146**, 1523 (1999)

Tie65 H.T. Tien, J. Phys. Chem. **69**, 350 (1965)

Tin94 C.H. Ting, *Proc. Topical Research Conf. On Low Dielectric Constant Interlayer Dielectric Constant Interlayer Dielectrics for High Performance Circuits*, SRC, Research Triangle Park, NC (1994)

Tse97	W-T. Tseng, Y-T. Hsieh, C-F. Lin, M-S. Tsai and M-S. Feng, J. Electrochem. Soc. **144**, 1100 (1997)
Wan97a	Y-L. Wang, J. Wu, C-W. Liu, T-C. Wang and J. Dun, Thin Solid Films **332**, 397(1997)
Wan97b	M.T. Wang, M.S. Tsai, C. Liu, W.T. Tseng, T.C. Chang, L.J. Chen and M.C. Chen, Thin Solid Films **308-309**, 518 (1997)
Wan97c	Y-L. Wang, C. Liu, S-T. Chang, M-S. Tsai, M-S. Feng and W-T. Tseng, Thin Solid Films **308-309**, 550 (1997)
Wes73	A.R.C. Westwood and N.H. Macmillan, in *Science of Hardness Testing*, ASM, Metals Park, OH, 377 (1973)
Wes81	A.R.C. Westwood, J.S. Ahearn and J.J. Mills, Colloids and Surfaces **2**, 1 (1981)
Wol86	S. Wolf and R.N. Tauber, *Silicon Processing for the VLSI Era*, Vol. 1, Lattice Press, CA, 188 (1986)
Woo97	J.A. Woollam Co., *Guide to using WVASE32*, Lincoln, NE (1997)
Wrs99	P. Wrschka, J. Hernandez, Y. Hsu, T.S. Kuan, G.S. Oehrlein, H.J. Sun, D.A. Hansen, J. King and M.A. Fury, J. Electrochem. Soc. **146**, 2689 (1999)
Xie96	Y. Xie and B. Bhushan, Wear **200**, p. 281 (1996)
Yak74	T. Yakovleva, L. Chunyayeva, A. Kovalenko and B. Belyavskaya, Sov. J. Opt. Technol. **41**, 44 (1974)
Yan97a	G-R. Yang, Y-P. Zhao, J.M. Neirynck, S.P. Murarka and R.J. Gutmann, J. Electron. Mater. 26, 935 (1997)
Yan97b	G-R. Yang, Y-P. Zhao, J.M. Neirynck, S.P. Murarka and R.J. Gutmann, J. Electrochem. Soc. **144**, 3249 (1997)
Yu92	C. Yu, P.C. Fazan, V.K. Mathews and T.T. Doan, Appl. Phys. Lett. **61**, 1344 (1992)
Yu93	T. Yu, C. Yu and M. Orlowski, Tech. Digest Int. Electron Devices Meeting **528**, 865 (1993)

BIOGRAPHICAL SKETCH

Uday Mahajan was born in 1973, in the city of Pune in India. After traveling around the country in his childhood as an "army brat", he joined the Indian Institute of Technology, Bombay. After four eventful years, he graduated in 1994 with a Bachelor of Technology in metallurgical engineering. After manufacturing trucks for one year in TELCO, he decided to pursue graduate studies in the United States. He joined the University of Cincinnati in September 1995, but the snow and the lack of a good football team caused him to transfer to the University of Florida in January 1996. He joined Dr. Rajiv Singh's group in January 1997 to work in the area of Chemical Mechanical Polishing. Besides being a diligent researcher, his other interests include ethanol, ornithology, travel and reading.

I certify that I have read this study and that in my opinion it conforms to acceptable standards of scholarly presentation and is fully adequate, in scope and quality, as a dissertation for the degree of Doctor of Philosophy.

Raj K.

Rajiv K. Singh, Chair
Professor of Materials Science
and Engineering

I certify that I have read this study and that in my opinion it conforms to acceptable standards of scholarly presentation and is fully adequate, in scope and quality, as a dissertation for the degree of Doctor of Philosophy.

Cammy R Abernathy

Cammy R. Abernathy
Professor of Materials Science
and Engineering

I certify that I have read this study and that in my opinion it conforms to acceptable standards of scholarly presentation and is fully adequate, in scope and quality, as a dissertation for the degree of Doctor of Philosophy.

Brij M. Moudgil

Brij M. Moudgil
Professor of Materials Science
and Engineering

I certify that I have read this study and that in my opinion it conforms to acceptable standards of scholarly presentation and is fully adequate, in scope and quality, as a dissertation for the degree of Doctor of Philosophy.

Stephen J. Pearton
Professor of Materials Science
and Engineering

I certify that I have read this study and that in my opinion it conforms to acceptable standards of scholarly presentation and is fully adequate, in scope and quality, as a dissertation for the degree of Doctor of Philosophy.

D. O. Shah

Dinesh O. Shah
Charles A. Stokes Professor of
Chemical Engineering

This dissertation was submitted to the Graduate Faculty of the College of Engineering and to the Graduate School and was accepted as partial fulfillment of the requirements for the degree of Doctor of Philosophy.

December, 2000

M. J. Ohanian
Dean, College of
Engineering

Winfred M. Phillips
Dean, Graduate School